

Multiwavelength analysis of three supernovae associated with gamma-ray bursts observed by GROND[★]

F. Olivares E.^{1,2}, J. Greiner¹, P. Schady¹, S. Klose³, T. Krühler^{4,★★}, A. Rau¹, S. Savaglio^{1,5}, D. A. Kann^{1,3}, G. Pignata², J. Elliott¹, A. Rossi^{3,★★★}, M. Nardini⁶, P. M. J. Afonso⁷, R. Filgas⁸, A. Nicuesa Guelbenzu³, S. Schmidl³, and V. Sudilovsky¹

¹ Max-Planck-Institut für extraterrestrische Physik, Giessenbachstraße 1, 85740 Garching, Germany
 e-mail: f.olivares.e@gmail.com

² Departamento de Ciencias Físicas, Universidad Andres Bello, Avda. Republica 252, Santiago, Chile

³ Thüringer Landessternwarte Tautenburg, Sternwarte 5, 07778 Tautenburg, Germany

⁴ Dark Cosmology Centre, Niels Bohr Institute, University of Copenhagen, Juliane Maries Vej 30, 2100 Copenhagen, Denmark

⁵ Physics Department, University of Calabria, Arcavacata, 87036 Rende, Italy

⁶ Università degli studi di Milano-Bicocca, Piazza della Scienza 3, 20126 Milano, Italy

⁷ American River College, Physics and Astronomy Dpt., 4700 College Oak Drive, Sacramento, CA 95841, USA

⁸ Institute of Experimental and Applied Physics, Czech Technical University in Prague, Horska 3a/22, 12800 Prague 2, Czech Republic

Received 21 May 2013 / Accepted 30 January 2015

ABSTRACT

Context. After the discovery of the first connection between γ -ray bursts (GRBs) and supernovae (SNe) almost two decades ago, tens of SN-like rebrightenings have been discovered and about seven solid associations have been spectroscopically confirmed to date.

Aims. We determine the luminosity, evolution, and origin of three SN rebrightenings in GRB afterglow light curves at $z \sim 0.5$ along with accurate determinations of the host-galaxy extinction. We estimate physical parameters of the SN explosions, such as synthesised ^{56}Ni mass, ejecta mass, and kinetic energy.

Methods. We employ GROND optical/NIR data and *Swift* X-ray/UV data to estimate the host-galaxy extinction by modelling the afterglow spectral energy distribution, to determine the SN luminosity and evolution, and to construct quasi-bolometric light curves. The latter are corrected for the contribution of the NIR-bands using data available in the literature and black-body fits. We employ Arnett's analytic approach to obtain the physical parameters of the explosion.

Results. The SNe 2008hw, 2009nz, and 2010ma observed by GROND exhibit 0.80, 1.15, and 1.78 times the optical (r' -band) luminosity of SN 1998bw, respectively. While SN 2009nz exhibits an evolution similar to SN 1998bw, SNe 2008hw and 2010ma show earlier peak times. The quasi-bolometric light curves (340–2200 nm) confirm the large luminosity of SN 2010ma (1.4×10^{43} erg s⁻¹), while SNe 2008hw and 2009nz reached a peak luminosity closer to that of SN 1998bw. The modelling indicates in ^{56}Ni masses of around 0.4–0.5 M_{\odot} .

Conclusions. By means of a very comprehensive data set, we found that the luminosity and the ^{56}Ni mass of SNe 2008hw, 2009nz, and 2010ma resembles those of other known GRB-associated SNe. These findings strengthens previous claims of GRB-SNe being brighter than stripped-envelope SNe unaccompanied by GRBs.

Key words. gamma-ray burst: individual: GRB 081007 – supernovae: individual: SN 2008hw – supernovae: individual: SN 2009nz – gamma-ray burst: individual: GRB 091127 – gamma-ray burst: individual: GRB 101219B – supernovae: individual: SN 2010ma

1. Introduction

Gamma-ray bursts (GRBs) and supernovae (SNe) correspond to the most energetic explosions in the Universe with a radiative energy release of about 10^{51-53} erg. Nowadays the observational evidence points towards the catastrophic deaths of massive stars, which are thought to give birth to both long GRBs (durations $\gtrsim 2$ s; Kouveliotou et al. 1993) and broad-lined (BL) type-Ic SNe after the collapse of their cores into a black hole (BH; Paczyński 1998a; Fryer et al. 1999; van Paradijs et al. 2000).

Known as the collapsar model (Woosley 1993; MacFadyen & Woosley 1999; Bromberg et al. 2012), the collapsing core of a very massive star can lead to the formation of a relativistic jet that will produce high-energy emission (Woosley 1993; Woosley & MacFadyen 1999) in the form of a GRB or an X-ray flash (XRF; Heise et al. 2001; Kippen et al. 2004; Sakamoto et al. 2008). The γ -ray emission itself lasts from a few tenths of a second to a few thousand seconds, is generated within the outflow at ultra-relativistic velocities, and is collimated into a jet (Zhang et al. 2009) that drills its way out of the star. The interactions between fireball shells with different speeds (“internal shocks”) are responsible for the prompt γ -ray emission. The multiwavelength afterglow (AG), detectable from radio throughout to X-rays up to months after the GRB (e.g. Kann et al. 2010, 2011), is explained by the synchrotron emission produced in the interaction between

[★] Appendices are available in electronic form at

<http://www.aanda.org>

^{★★} Present address: European Southern Observatory, Alonso de Córdova 3107, Vitacura, Casilla 19001, Santiago 19, Chile.

^{★★★} Present address: INAF–IASF Bologna, Area della Ricerca CNR, via Gobetti 101, 40129 Bologna, Italy.

the circumburst material and the relativistic outflow (“external shocks”; see [Zhang & Mészáros 2004](#), for a review).

In principle, the energy transferred to the envelope should also be capable of causing the ejection of the stellar envelope ([Burrows 2000](#); [Heger et al. 2003](#)). However, it is unclear how or even if there is always enough energy for the SN explosion (“fall-back” events e.g. [Fryer et al. 2007](#), and references therein). Moreover, it is unknown exactly to what extent the progenitors have to lose their envelope to produce a GRB. However, it is generally accepted that type-Ib and type-Ic SNe are formed from evolved high-mass progenitors like Wolf-Rayet (WR) stars, which have liberated their outer shells through (1) pre-SN stellar winds; (2) mass transfer to a binary companion due to Roche-lobe overflow; or (3) a combination of both processes. The stellar explosion is then referred to as a “stripped-envelope” SN (SE SN; [Clocchiatti & Wheeler 1997](#)). The end result of a GRB-SN explosion would correspond to a compact remnant, either a neutron star (NS; [Baade & Zwicky 1934](#)) or a BH ([Arnett 1996](#)). To date, long GRBs have only been associated with type-Ic BL SNe, which are those lacking H ([Minkowski 1941](#)) and He lines ([Filippenko 1997](#)) and showing expansion velocities of the order of $20\,000\text{ km s}^{-1}$ (for reviews on the GRB-SN connection, see [Woosley & Bloom 2006](#) and [Hjorth & Bloom 2012](#)).

The first and most representative case of the GRB-SN connection is the association of SN 1998bw with the underluminous GRB 980425 ([Kippen 1998](#); [Sadler et al. 1998](#)). Although initially controversial ([Galama et al. 1998](#); [Pian et al. 1998](#)), the physical association between these events was supported on temporal ([Iwamoto et al. 1998](#)) and spatial grounds ([Pian et al. 2000](#); [Kouveliotou et al. 2004](#)). Five years later, the association of GRB 030329 with SN 2003dh was clearly identified through spectra showing both the AG and SN counterparts ([Hjorth et al. 2003](#); [Kawabata et al. 2003](#); [Stanek et al. 2003](#); [Matheson et al. 2003](#)) and became a solid piece of evidence in favour of the GRB-SN connection. There have been a number of other spectroscopic associations¹, which in the literature are also dubbed “hypernovae” (HNe; [Paczynski 1998b](#); [Hansen 1999](#)) given their high luminosities. Because of their high energetics, HNe produce $\geq 0.2 M_{\odot}$ of ^{56}Ni , are thought to have very massive progenitors, and are often connected to BH formation ([Nomoto et al. 2010](#); [Stritzinger et al. 2009](#)).

Late-time rebrightenings in AG light curves have been interpreted as SN signals, e.g. GRBs 970228 ([Galama et al. 2000](#); [Reichart et al. 2000](#)), 011121 ([Bloom et al. 2002](#); [Greiner et al. 2003](#)), 020405 ([Price et al. 2003](#); [Masetti et al. 2003](#)), 041006 ([Stanek et al. 2005](#); [Soderberg et al. 2006](#)), 060729, and 090618 (the latter two in [Cano et al. 2011](#)) to mention a few. These photometric bumps are consistent in terms of colour, timing, and brightness with those expected for the GRB-SN population

([Zeh et al. 2004](#); [Ferrero et al. 2006](#)), but they are usually at faint apparent magnitudes, which hampers the spectroscopic identification. However, the SN counterpart can be as bright as $M_V = -19.8$ mag for SN 2003lw ([Malesani et al. 2004](#)). These rebrightenings have been detected in AG light curves out to redshifts of ~ 1 (e.g. [Masetti et al. 2005](#); [Della Valle et al. 2003](#)) owing to the sensitivity of current ground-based telescopes dedicated to follow-up observations. A handful of sample studies of GRB-SNe (including bumps not spectroscopically identified) have analysed the luminosity distribution, the light-curve morphology, and the explosion physical parameters such as kinetic energy (E_k), ejected mass (M_{ej}), and ^{56}Ni mass (M_{Ni} ; [Richardson 2009](#); [Thöne et al. 2011](#); [Cano 2013](#)). They concluded that GRB-SNe are in general brighter than the local sample of SE SNe, except for cases of exceptionally bright type-Ic SNe (e.g. SN 2010ay, [Sanders et al. 2012](#); SN 2010gx, [Pastorello et al. 2010](#)). Regarding light-curve morphology, [Stanek et al. \(2005\)](#) and more recently [Schulze et al. \(2014\)](#) claim to have found a correlation between brightness and light-curve shape, which was also confirmed by [Cano \(2014\)](#) using a larger sample and including the appropriate K corrections. This strengthens the use of GRB-SNe as standard candles for cosmology (see also recent studies by [Li & Hjorth 2014](#); [Cano & Jakobsson 2014](#); and [Li et al. 2014](#)). While more than two dozen photometric bumps in AG light curves have been presented as SN rebrightenings (e.g. [Richardson 2009](#)), so far only seven have been confirmed through high signal-to-noise spectra: SNe 1998bw, 2003dh, 2003lw, 2006aj, 2010bh, 2012bz, 2013dx, and 2013cq.

The energy injection of a newly-formed NS characterised by rapid rotation and strong magnetic field (so-called “magnetar”) provides an alternative scenario for GRB-SNe. Here the SN is powered by the dipole-field strength of the magnetar (e.g. [Woosley 2010](#); [Dessart et al. 2012](#)). Magnetars have been linked to the GRB emission too because their outflows can explain the energetics of long-duration GRBs (e.g. [Bucciantini et al. 2009](#); [Metzger et al. 2011](#)). Moreover, the E_k of GRB-SNe ($\sim 10^{52}$ erg) is fairly consistent with the maximum rotational energy of a NS with a period of 1 ms ([Mazzali et al. 2006a](#)). The GRB-SN zoo is claimed to be entirely produced by magnetars and driven by the SN rather than by the GRB jet ([Mazzali et al. 2014](#)).

Three detected SNe associated with GRB counterparts are the main focus of this paper: SNe 2008hw (GRB 081007), 2009nz (GRB 091127), and 2010ma (GRB 101219B). The acquisition, reduction, and calibration of the multiwavelength data are described in Sect. 2. The corresponding analysis is presented in Sect. 3 along with further discussion in Sect. 4. Finally, we summarise our conclusions in Sect. 5.

2. Data

For the three objects of interest, the data was obtained by the X-Ray Telescope (XRT; [Burrows et al. 2005](#)) and the Ultra-Violet Optical Telescope (UVOT; [Romig et al. 2005](#)), both on board the *Swift* satellite ([Gehrels et al. 2004](#)), and by the Gamma-Ray burst Optical and Near-infrared Detector (GROND; [Greiner et al. 2007, 2008](#)), the seven-channel imager mounted on the MPG 2.2-m telescope at La Silla, Chile. The whole data set comprises X-ray photometry and spectra from 0.2–10 keV, UV/optical photometry in the *uvw2 uvw1 u b v* filters, and optical/near-infrared (NIR) photometry in the *g' r' i' z' J H K_s*-bands, spanning four orders of magnitude in the energy spectrum.

The UVOT/XRT data retrieval and the GROND/UVOT methodology towards the final photometry are detailed in

¹ These also showed BL features in their spectra: GRB 021211/SN 2002lt ([Della Valle et al. 2003](#)), GRB 031203/SN 2003lw ([Malesani et al. 2004](#)), GRB 050525A/SN 2005nc ([Della Valle et al. 2006](#)), GRB 060218/SN 2006aj ([Pian et al. 2006](#); [Modjaz et al. 2006](#); [Sollerman et al. 2006](#)), GRB 081007/SN 2008hw ([Della Valle et al. 2008](#); [Jin et al. 2013](#)), GRB 091127/SN 2009nz ([Berger et al. 2011](#)), GRB 101219B/SN 2010ma ([Sparre et al. 2011a](#)), GRB 111211A ([de Ugarte Postigo et al. 2012](#)), GRB 100316D/SN 2010bh ([Chornock et al. 2010](#); [Bufano et al. 2012](#)), GRB 120422A/SN 2012bz ([Melandri et al. 2012](#); [Schulze et al. 2014](#)), GRB 120714B/SN 2012eb ([Klose et al. 2012a,b](#)), GRB 130215A ([de Ugarte Postigo et al. 2013](#); [Cano et al. 2014](#)), GRB 130427A/SN 2013cq ([Xu et al. 2013](#)), GRB 130702A/SN 2013dx ([Schulze et al. 2013](#)), GRB 130831A/SN 2013fu ([Klose et al. 2013](#); [Cano et al. 2014](#)), and GRB 140606B ([Perley et al. 2014](#)).

Table 1. GROND sample of GRB-associated SNe.

GRB	SN	RA(J2000) [^h : ^m : ^s]	Dec(J2000) [[°] : ['] : ^{''}]	z	d^a [Mpc]	$A_{V,\text{Gal}}^b$ [mag]	$N_{\text{H,Gal}}^c$ [10^{20} cm^{-2}]	Refs.
081007	2008hw	22:39:50.40	-40:08:48.8	0.530	2885	0.05	1.4	1
091127	2009nz	02:26:19.87	-18:57:08.6	0.490	2628	0.12	2.8	2
101219B	2010ma	00:48:55.35	-34:33:59.3	0.552	3022	0.06	3.1	3

Notes. ^(a) The luminosity distances are computed using the Λ CDM cosmological model ($\Omega_M = 0.27$, $\Omega_\Lambda = 0.73$, and $H_0 = 74.2 \text{ km s}^{-1} \text{ Mpc}^{-1}$; Riess et al. 2009) and the redshifts corrected by the local velocity field (Mould et al. 2000). ^(b) The Galactic foreground extinction values are taken from the dust maps of Schlegel et al. (1998). ^(c) The absorption column densities are taken from the Galactic HI maps of Kalberla et al. (2005).

References. Redshifts are taken from (1) Berger et al. (2008); (2) Vergani et al. (2011); (3) Sparre et al. (2011b).

Table 2. GROND photometry of the host galaxies.

GRB	SN	g'	r'	i'	z'	J	H	K_s
081007	2008hw	24.66 ± 0.11	24.49 ± 0.11	24.08 ± 0.19	23.96 ± 0.24	>22.0	>21.1	>20.1
091127	2009nz	24.08 ± 0.09	23.45 ± 0.06	22.85 ± 0.07	22.95 ± 0.08	>21.7	>21.4	>19.9
101219B	2010ma	>25.4	>25.2	>24.5	>24.5	>22.2	>22.0	>20.2

Notes. The host-galaxy magnitudes are all corrected for the corresponding Galactic foreground extinction. The upper limits were derived from the deepest observation available showing no detection and are quoted at the 3σ confidence level.

Olivares E. et al. (2012). Optical image subtraction of the host galaxy was performed for GRB 081007/SN 2008hw and GRB 091127/SN 2009nz. All data presented are corrected for the Galactic foreground reddening $E(B - V)_{\text{Gal}}$ in the direction of the burst (Schlegel et al. 1998). The reddening is transformed to the extinction $A_{V,\text{Gal}}$, assuming a ratio of total to selective absorption of $R_{V,\text{Gal}} = 3.1$ from the Milky-Way (MW) reddening law. The final GROND photometry is presented in Appendix A. All magnitudes throughout the paper are in the AB system.

3. Three GRB-associated SNe detected by GROND

Table 1 presents a sub-sample of GRBs with late-time optical SN rebrightenings in their AG light curves, all of them observed by GROND. Deep late-time observations were carried out for each of them to constrain the contribution from their host galaxies. If the host was detected, we performed image subtraction. Table 2 presents the resulting photometry for those host galaxies. In the following, observational facts and general properties of each event are summarised from the literature. If possible, mass estimates are derived from the spectral energy distributions (SEDs) of the host galaxies using the hyperZ code (Bolzonella et al. 2000) and a library of galaxy spectral templates extinguished by the different reddening laws.

GRB 081007/SN 2008hw. The *Swift*/BAT (Barthelmy et al. 2005) discovered GRB 081007 at 05:23:52 UT on 2008 October 7 (Baumgartner et al. 2008). The prompt emission had a duration of $T_{90} \approx 10 \text{ s}$ and a soft spectrum with $E_{\text{peak}} \lesssim 30 \text{ keV}$ (Markwardt et al. 2008). The redshift of $z = 0.5295$ was found by Berger et al. (2008) through optical spectroscopy. A subsequent optical spectrum taken 17 days after the burst shows broad features indicative of an emerging SN, which was thereafter classified as Type I (no hydrogen lines) and named SN 2008hw (Della Valle et al. 2008). The SN bump was also reported as a flux excess with respect to the AG (Soderberg et al. 2008). The GROND photometry of the host galaxy (Table 2) from August 31, September 30, and October 21, 2011, yields a stellar-mass range of $M_\star \sim 10^{8-9} M_\odot$, which is compatible

with the population of GRB hosts (Savaglio et al. 2009). Using appropriate transformation equations², our host magnitudes are somewhat brighter but marginally consistent with the measurements published by Jin et al. (2013) of $R_C > 24.67$ and $I_C = 24.29 \pm 0.20 \text{ mag}$ at $\sim 87 \text{ d}$ after the GRB.

GRB 091127/SN 2009nz. At 23:25:45 UT on 2009 November 27, the *Swift*/BAT was triggered by GRB 091127 (Troja et al. 2009). The γ -ray emission lasted for $T_{90} = 7.1 \text{ s}$ and showed a soft spectrum (Stamatikos et al. 2009; Troja et al. 2012). A redshift of $z = 0.490$ was obtained from optical spectroscopy (Cucchiara et al. 2009; Thöne et al. 2009). Observations by Konus-Wind confirmed the results from the *Swift*/BAT (Golenetskii et al. 2009) and additionally yielded an energy release typical for cosmological GRBs ($E_{\gamma,\text{iso}} \sim 10^{52} \text{ erg}$). The optical AG was confirmed with GROND observations (Updike et al. 2009) adding NIR detections. The full analysis of the GROND AG light curve was presented in Filgas et al. (2011). The SN classification became official based on the photometric SN bump (Cobb et al. 2010a,b) and spectroscopy was published later showing BL features (Berger et al. 2011). Photometry depicting the SN rebrightening was published in Cobb et al. (2010c) and Vergani et al. (2011). Using the host-galaxy detections in GROND optical imaging (October 31, 2010) and in NIR photometry from Vergani et al. (2011), a stellar mass of $M_\star = 10^{8.4} M_\odot$ is obtained. This value falls in the low-mass end of the observed distribution of GRB host masses (Savaglio et al. 2009) and is compatible with the stellar mass computed by Vergani et al. (2011).

GRB 101219B/SN 2010ma. At 16:27:53 UT on 2010 December 19, the *Swift*/BAT discovered GRB 101219B (Gelbord et al. 2010). The BAT burst lasted $T_{90} \approx 34 \text{ s}$ (Cummings et al. 2010) and consisted of a spectrum with $E_{\text{peak}} \approx 70 \text{ keV}$ as observed by *Fermi*/GBM (van der Horst 2010). The SN discovery was first reported photometrically

² <http://www.sdss.org/dr7/algorithms/sdssUBVRITransform.html>

Table 3. Parameters of the AG component and goodness of the light-curve modelling.

GRB	α_1	t_{break} [days]	η	α_2	χ^2/μ
081007	-0.66 ± 0.01	0.91 ± 0.05	15 fixed	-1.40 ± 0.05	1.5
091127	-0.38 ± 0.01^a	0.34 ± 0.01^a	1.3 ± 0.1^a	-1.63 ± 0.02	1.4
101219B	-1.01 ± 0.01	1.8

Notes. The primary power-law slope is α_1 . In case of a break in the light curve, a secondary slope α_2 along with the break time t_{break} and break smoothness parameter η are introduced. The ratio χ^2/μ is computed in the multiple-component fitting procedure, which includes AG plus SN modelling. See Table 4 for the SN parameters. ^(a) Parameters were taken from the fitting of the full GROND r' -band light curve by Filgas et al. (2011) except α_2 , which was fitted by a single power law using the data only presented in Fig. 2.

Table 4. Parameters of the SN component with respect to SN 1998bw templates.

SN	GRB	Stretch factor (s)	g'	Luminosity ratio (k) ^a		
				r'	i'	z'
2008hw	081007	0.85 ± 0.11	<0.90	0.80 ± 0.10	0.65 ± 0.08	0.69 ± 0.10
2009nz	091127	1.03 ± 0.04	<1.21	1.15 ± 0.09	0.96 ± 0.14	0.73 ± 0.12
2010ma ^b	101219B	0.76 ± 0.10	0.85 ± 0.17	$1.78^{+0.08}_{-0.17}$	1.36 ± 0.09	0.63 ± 0.09

Notes. ^(a) Luminosity ratios are all corrected for Galactic and host-galaxy extinction. The latter correction is taken from the AG SED fitting in Sect. 3.2. ^(b) No host-galaxy contribution was assumed. See text for estimations including host emission.

by Olivares E. et al. (2011) along with a redshift estimation assuming the brightness of SN 1998bw for the rebrightening ($z = 0.4\text{--}0.7$). The spectroscopic confirmation of SN 2010ma came later by Sparre et al. (2011a) along with the redshift determination of $z = 0.55185$ from weak Mg absorption lines. The spectroscopy led to further analysis by Sparre et al. (2011b) that shows broad-line features characteristic of GRB-SNe. Late-time GROND observations on September 30, 2011, show no signal of a host galaxy down to deep limits (Table 2), therefore no image-subtraction procedure was performed. These upper limits imply a stellar mass for the host galaxy of $M_\star \lesssim 10^{9.2} M_\odot$, which corresponds to the low-mass half of observed GRB host mass distribution and is marginally compatible with the Small Magellanic Cloud (SMC).

3.1. Multicolour light-curve fitting

After image subtraction of the host galaxy in the cases where it was detected (Table 2), the light curves were fitted simultaneously using one or two power-law components ($F_\nu \sim t^\alpha$) and templates of SN 1998bw, where corrections due to redshift and Galactic foreground extinction were taken into account (see Zeh et al. 2004, for details on the fitting of SN 1998bw templates). Simultaneous modelling consists of unique power-law slopes α_1 , α_2 , and SN-template stretch factor s for all bands. The ratio between the luminosity of the observed SN and that of SN 1998bw (luminosity ratio k ; Zeh et al. 2004) represents the free brightness parameter, which was fitted to the light curves only corrected for Galactic extinction. Therefore, the luminosity ratios are then corrected for the host-galaxy extinction $A_{V,\text{host}}$ determined by the SED modelling (see Sect. 3.2). The modelling is described in detail below for each event and summarised in Tables 3 and 4.

GRB 081007/SN 2008hw. Figure 1 shows that the light curves in all seven bands are well modelled using a broken power law (Beuermann et al. 1999). The $g'r'i'z'$ photometry has been image-subtracted to remove the host-galaxy flux. The X-ray light curve from the *Swift*/XRT was included in the fitting to constrain the decay after the break, where there is only a single

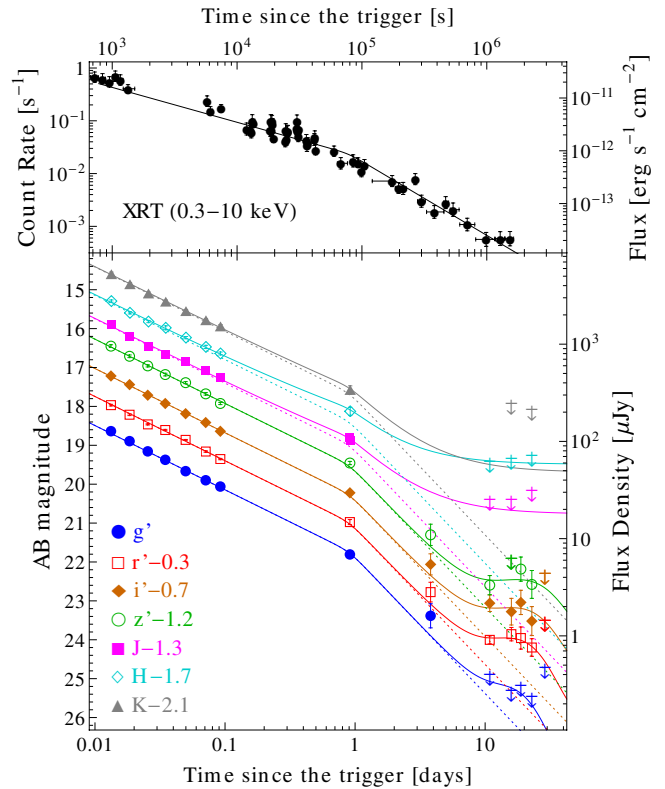


Fig. 1. Multicolour light curves of GRB 081007/SN 2008hw corrected for Galactic extinction as observed by the *Swift*/XRT (upper panel) and GROND (lower panel). Filled circles represent detections and arrows are upper limits. Solid lines correspond to the overall fits and dotted lines to the AG component. For clarity, light curves were shifted along the magnitude axis. Shallow upper limits are not shown (see Table A.1 for the complete data set).

optical epoch. For the $r'i'z'$ -bands, it was necessary to add an SN component with a luminosity about 65–80% that of SN 1998bw (see Table 4). Because of the JHK_s flux excesses with respect to the broken power law at roughly one day after

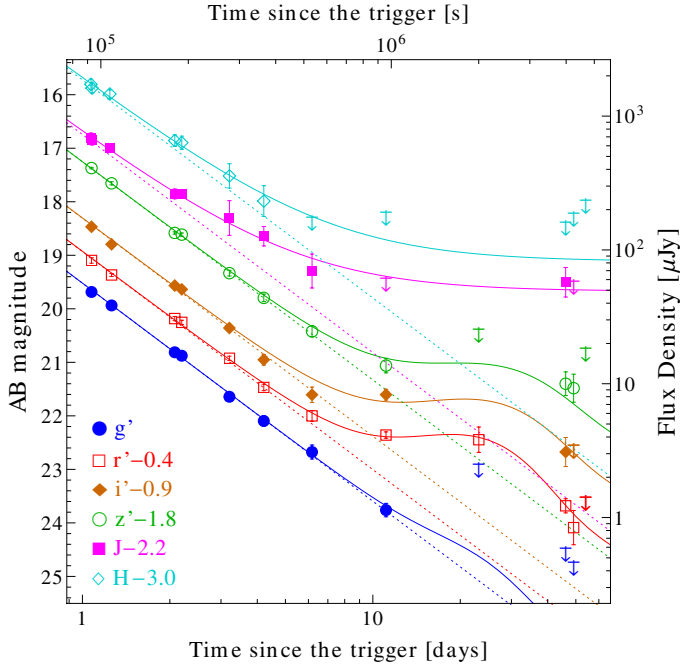


Fig. 2. Multicolour GROND light curves of GRB 091127/SN 2009nz corrected for Galactic extinction. We only employed data after day one. The symbol and line coding is the same as Fig. 1 as well as the vertical shift for clarity.

the burst, a constant component was included in the modelling for these bands. The g' -band upper limit is strongly affected by absorption of metal lines and wavelength extrapolation of the SN 1998bw template (e.g. the case of SN 2009nz due to high redshift). Jin et al. (2013) report a luminosity of 50% that of SN 1998bw, however, without accounting for the significant host extinction (see Sect. 3.2).

GRB 091127/SN 2009nz. Figure 2 presents the light curves of the AG in six bands. The $g'r'i'z'$ photometry has been image-subtracted to remove the host-galaxy flux. All are well fitted by a single power law, which needed a SN component for the $g'r'i'z'$ -bands. No K_s -band observations were obtained for this event (Filgas et al. 2011). The brightest host galaxy allowed by the data was included in the model for JH at late times (see Table 2). The k and s values reflect strong similarities to SN 1998bw in the $r'i'$ -bands. At the redshift of SN 2009nz ($z = 0.490$), the g' -band is probing wavelengths centred at $\sim 3000 \text{ \AA}$, where the flux is strongly affected by absorption-line blanketing of metals, and so the intensity can differ from SN to SN. Moreover, since the U -band, the bluest band from which the SN 1998bw templates are constructed, is sensitive $\gtrsim 3000 \text{ \AA}$, extrapolations dominate the g' -band template. Also, given the non-detections after day 12, we derived an upper limit of $k_{g'} < 1.21$ from the fitting (Table 4).

GRB 101219B/SN 2010ma. Figure 3 shows the GROND light curves of the optical counterpart. The SN bump is clearly seen in the $r'i'z'$ -bands, however, it is less significant in the g' -band. At the redshift of the event, the g' -band actually probes the UV regime, therefore, the lower g' -band SN luminosity is explained by a combination of both the wavelength extrapolation of the template and the UV line blanketing by metals. Even though the host galaxy remained undetected, it may explain the flux excess 35 days after the burst in the r' -band (dashed

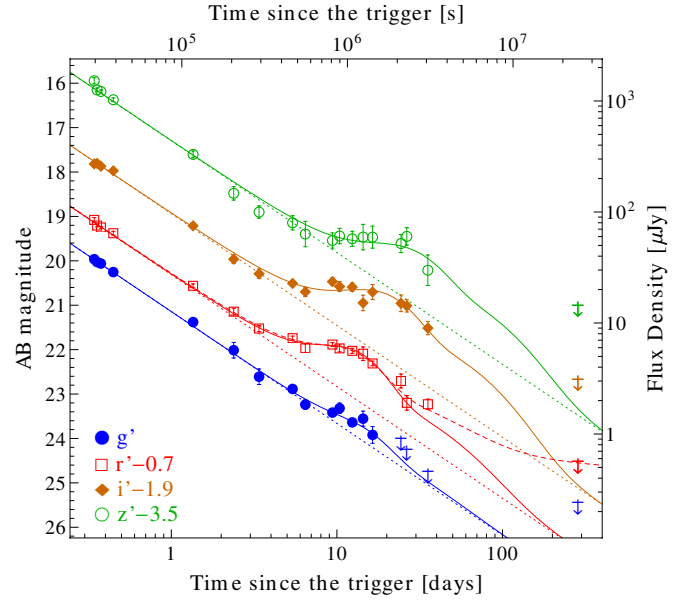


Fig. 3. Multicolour GROND light curves of GRB 101219B/SN 2010ma corrected for Galactic extinction. The symbol and line coding is the same as Fig. 1 as well as the vertical shift for clarity. The red dashed line represents a model with an extra host-galaxy component.

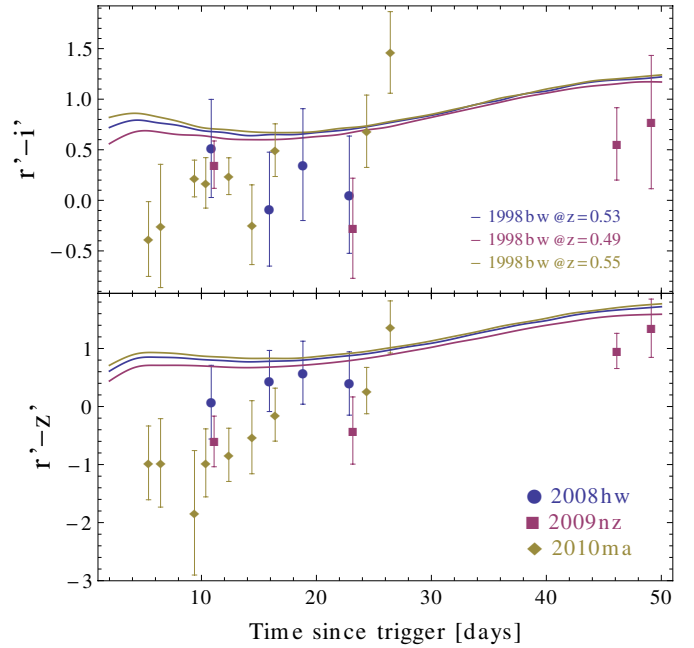


Fig. 4. Colour curves corrected for the total extinction of SNe 2008hw (blue circles), 2009nz (purple squares), and 2010ma (gold diamonds) after AG and host subtraction. Blue, purple, and gold solid lines are computed from the templates of SN 1998bw at redshifts of SNe 2008hw, 2009nz, and 2010ma, respectively.

line in Fig. 3). The k value would decrease $\sim 14\%$ in this case. Therefore, the lower error in $k_{r'}$ was increased to match the 3σ lower limit when assuming the brightest host component possible (Table 4). We note that the k value for the z' -band is smaller compared to the bluer bands. Along with the differences in the SN luminosity ratio among all bands, this indicates that the colours of SN 2010ma are different from those of SN 1998bw. Figure 4 shows the colour curves of the three SNe analysed

Table 5. Parameters of the SED modelling of the AG.

GRB	β_X	$A_{V,\text{host}}$ [mag]	E_{break} [eV]	$N_{\text{H},\text{host}}$ [10^{21} cm^{-2}]	χ^2/μ
081007	0.97 ± 0.09	0.68 ± 0.08 (SMC)	37^{+54}_{-12}	5.6 ± 0.7	1.1
091127 ^a	0.748 ± 0.004	<0.03 (LMC)	2.6–29.9	0.32 ± 0.06	1.1
101219B	1.12 ± 0.01	0.12 ± 0.01 (SMC)	9.0 fixed	0.6 ± 0.3	0.8

Notes. Obeying the fireball model for GRB AGs, the high-energy (β_X) and the low-energy (β_{opt}) spectral indexes are correlated by $\beta_X = \beta_{\text{opt}} + 0.5$ for $E_{\text{break}} \approx E_{\text{cooling}}$, where the latter comes from the cooling frequency of the electrons, except in the case of GRB 091127 where β_{opt} varies in the range 0.25–0.62. ^(a) The quoted values of β_X , $N_{\text{H},\text{host}}$, and reduced χ^2 are computed from the simultaneous best fit to all eight GROND/XRT SEDs by Filgas et al. (2011). The E_{break} range comes from an observed evolution of β_{opt} . The $A_{V,\text{host}}$ upper limit was taken from Schady et al. (2012).

compared against the templates of SN 1998bw, where the bluer emission of SN 2010ma is significant at early times.

3.2. Spectral energy distributions

Using the available X-ray data from the *Swift*/XRT, the UV/optical data from the *Swift*/UVOT, and the optical/NIR data from GROND, we constructed a single AG SED per event with the main purpose of determining the extinction along the line of sight through the host galaxy. The SED modelling was performed similar to Greiner et al. (2011), and the results are presented in Table 5.

Note that the AG may probe a slightly different line of sight than the SN photosphere. If anything, the extinction for the SN should be larger than for the AG because the AG forms further out, where the material ejected by the GRB hits the circumstellar medium. In the standard fireball shock model, this radius is about 10^{17} cm (and even larger for low-luminosity events; Molinari et al. 2007). Moreover, dust can be formed in the SN ejecta, although significant amounts do not form on such short timescales (e.g. Smith et al. 2012). Therefore, we considered that the extinction determined through the AG SED is valid for the SN component as well. The following corresponds to a description of the SED fitting for each of the rebrightenings.

GRB 081007/SN 2008hw. To include contemporaneous *Swift*/UVOT data, the second GROND epoch was chosen to study the broad-band SED of GRB 081007 presented in Fig. 5. From the UVOT, upper limits in the UV-bands are included, which help to constrain the host-galaxy extinction. The time-integrated *Swift*/XRT spectrum was interpolated to the epoch of the UV/optical observations. The resulting values of host-galaxy extinction and its corresponding statistical uncertainty are consistent with those computed by Covino et al. (2013), and for the GROND filters we obtain $A_{g',\text{host}} = 1.39 \pm 0.16$, $A_{r',\text{host}} = 0.99 \pm 0.12$, $A_{i',\text{host}} = 0.77 \pm 0.09$, $A_{z',\text{host}} = 0.63 \pm 0.07$, $A_{J,\text{host}} = 0.38 \pm 0.04$, $A_{H,\text{host}} = 0.24 \pm 0.03$, and $A_{K,\text{host}} = 0.14 \pm 0.02$ in the observer's frame, all in units of magnitude. These values were used to correct the SN luminosity ratios shown in Table 4.

GRB 091127/SN 2009nz. The broad-band SEDs of the early AG of GRB 091127 were presented by Filgas et al. (2011) using the GROND data. A detailed analysis by Schady et al. (2012) includes *Swift*/UVOT and GROND data and constrains the host-galaxy extinction, which results in $A_{V,\text{host}} < 0.03$ mag. The SED parameters are shown in Table 5.

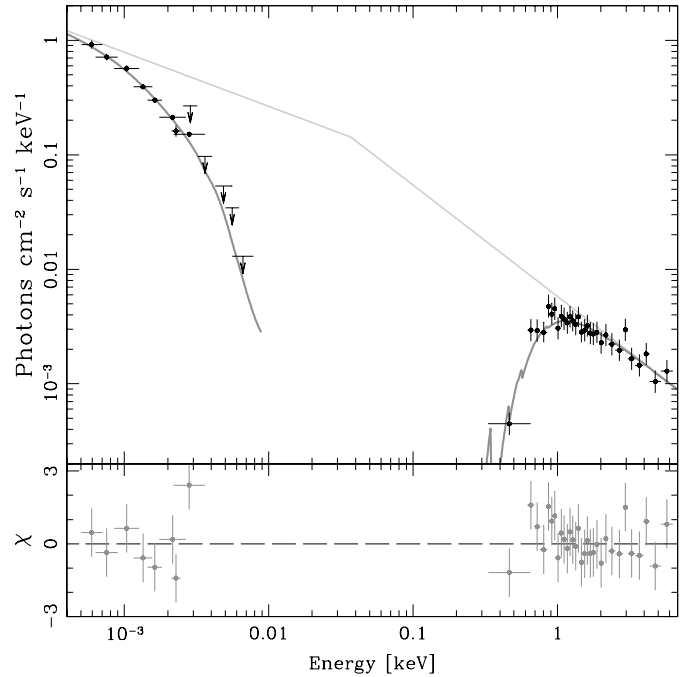


Fig. 5. Broad-band AG SED of GRB 081007 at 1.6 ks after trigger. The arrows are 3σ upper limits. The best-fit model (thick line) is an extinguished broken power law. The thin line represents the unextinguished model. The residuals are in units of χ (lower panel).

GRB 101219B/SN 2010ma. Using GROND, XRT, and UVOT data combined, the AG SED of GRB 101219B was constructed at 9 h after the burst. Figure 6 shows a broken power law as the best fit. The values of the required host-galaxy extinction for the GROND filters and their corresponding statistical uncertainty in the observer's frame are $A_{g',\text{host}} = 0.25 \pm 0.03$, $A_{r',\text{host}} = 0.18 \pm 0.02$, $A_{i',\text{host}} = 0.14 \pm 0.02$, $A_{z',\text{host}} = 0.11 \pm 0.01$, $A_{J,\text{host}} = 0.07 \pm 0.01$, $A_{H,\text{host}} = 0.04 \pm 0.01$, and $A_{K,\text{host}} = 0.026 \pm 0.003$, all in units of magnitude.

3.3. Calculation and modelling of the bolometric light curves

To isolate the SN from the AG evolution, the light-curve models computed in Sect. 3.1 were employed. The AG contribution was calculated from the model for the epochs when the SN bump was observed and it was subtracted from the light curves for each filter. The uncertainties in the model were appropriately propagated to the final magnitude errors. After the AG subtraction, quasi-bolometric light curves were computed for each of the three events by numerically integrating the monochromatic

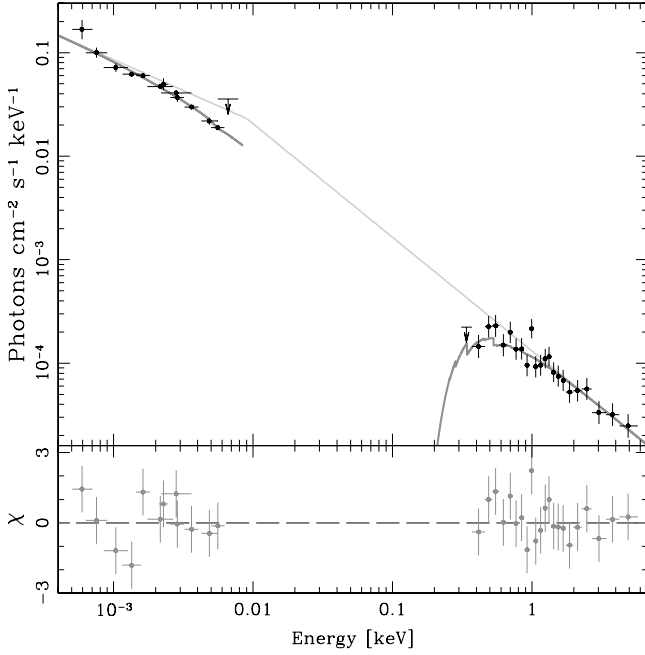


Fig. 6. Broad-band AG SED of GRB 101219B at 9.0 h after trigger. The symbols, line coding, and panels are the same as in Fig. 5.

fluxes in the wavelength range from 340 to 700 nm. The redshift-based luminosity distances in Table 1 were employed to transform observed into absolute flux. The total uncertainty in the luminosity distance is about 10% and has not been included in the quasi-bolometric light curves.

3.3.1. NIR bolometric correction

The NIR luminosity proves critical when estimating the bolometric flux and, consequently, the physical parameters of the explosion obtained via the quasi-bolometric flux. However, SNe 2008hw, 2009nz, and 2010ma remained undetected in the *JHK*-bands. To account for the NIR flux of these SNe, we proceeded with two different methods. First of all, we defined the NIR flux from 700 to 2200 nm in the rest frame and the quasi-bolometric flux from 340 to 2200 nm. The quantity to be estimated via the two methods is the ratio between the NIR flux and the quasi-bolometric flux, as defined above.

The first method consisted in estimating the NIR fraction of the quasi-bolometric flux using the observed NIR data available in the literature. With the optical/NIR photometry, we computed the ratio between the NIR and the quasi-bolometric fluxes for the GRB-SNe 1998bw (Kocevski et al. 2007) and 2006aj (Patat et al. 2001), and for the type-Ib/c SNe 2002ap (Foley et al. 2003; Yoshii et al. 2003), 2007uy (Roy et al. 2013), and 2008D (Modjaz et al. 2009). We show the observed NIR fractions in the upper panel of Fig. 7 along with a quadratic-polynomial fit for each SN. For each fit, we also obtained the corresponding uncertainty as a function of time. Taking the weighted average per time bin (5 days width, $t_i = 1$ d), we derived the joint evolution of the NIR fraction for the five SNe. The non-weighted rms was taken as the 1σ error. Only the first time bin uses data from a single event and the error here is approximated by the uncertainty in the individual polynomial fit. The binned NIR fraction was interpolated using quadratic polynomials to retrieve values for a given time and to plot the grey contours in Fig. 7. The SNe 2007uy and 2008D do not contribute much to the weighted

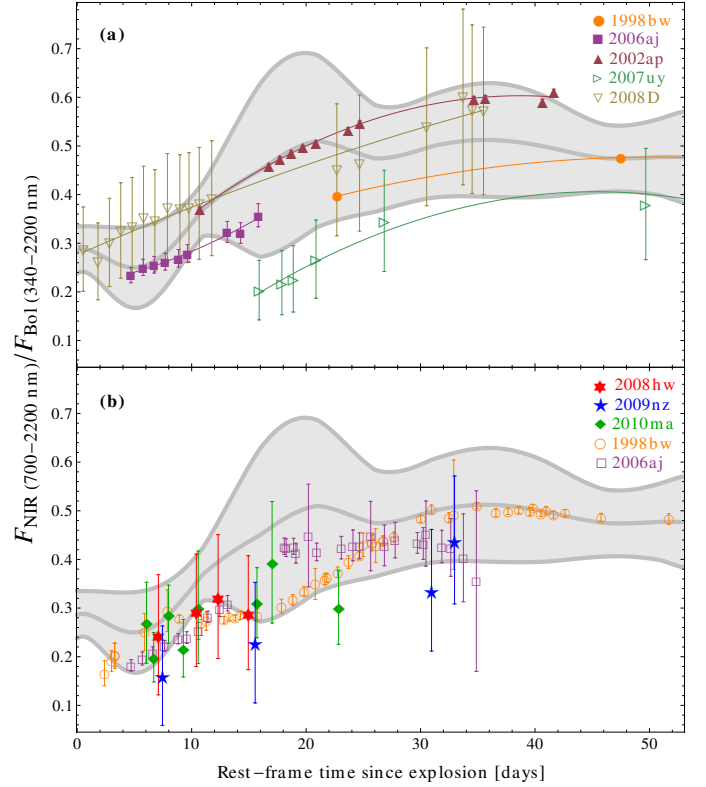


Fig. 7. NIR fraction (700–2200 nm) of the quasi-bolometric flux (340–2200 nm) for SE SNe. **a)** The values derived using optical/NIR data of five SE SNe are fitted separately (coloured solid lines), averaged, and interpolated (grey solid line and 1σ contours). **b)** The estimations from the BB fits to optical data are shown for five GRB-SNe along with the contours from the top panel. See main text for the references of the data sources.

average, because their host extinction is large and highly uncertain (0.3–0.5 mag; Mazzali et al. 2008; Roy et al. 2013).

The second method assumes that the SN atmosphere at early phases resembles a cooling black body (BB; e.g. Arnett 1982; Filippenko 1997; Dessart & Hillier 2005). We defined a simple BB model with the temperature and a flux normalisation as free parameters. Then, we modelled the SN SEDs constructed using $g'r'i'z'$ data at each epoch. The results of the fitting procedure are shown in Appendix C. We obtain colour temperatures decreasing with time and consistent with other SE SNe (e.g. Folatelli et al. 2014). The extrapolation into the NIR range delivered NIR fractions plotted in the lower panel of Fig. 7 with uncertainties between 0.05 and 0.13. The increasing NIR flux with time is consistent with the scenario of the cooling envelope. We repeated this procedure for the optical data of SNe 1998bw (*UBVRI*; Galama et al. 1998) and 2006aj (*UBVR*; Pian et al. 2006; Sollerman et al. 2006) with results that are consistent with those for SNe 2008hw, 2009nz, and 2010ma. Moreover, the 1σ contours from the first method (grey-shaded region) are compatible with the all BB estimates derived using solely optical photometry.

The final NIR correction applied to the optical data was the average value between the estimates from the available NIR data for GRB-SNe and the estimates from the BB fits. A conservative proxy of the NIR-fraction error was chosen to be the largest among the difference between the two estimates and their respective errors. Errors fluctuate between 0.07 and 0.22. We note that the NIR correction implies *JHK* magnitudes at maximum consistent with the upper limits presented

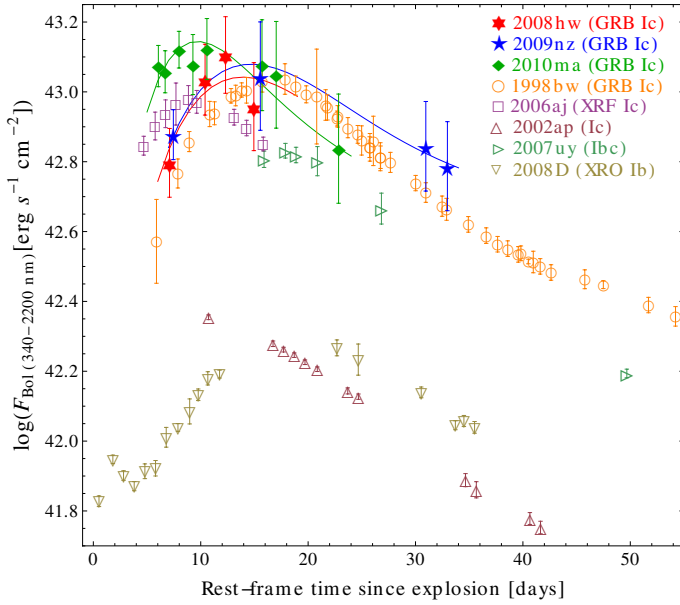


Fig. 8. Quasi-bolometric (340–2200 nm) light curves of SNe 2008hw (red six-pointed stars), 2009nz (blue five-pointed stars), and SN 2010ma (green filled diamonds). The analytic model is shown for each SN with its respective colour (details in Sect. 3.3). A handful of other type-Ib/c SNe are shown for comparison (see main text for the references).

in Figs. 1–3. For instance, the brightest magnitudes derived from the NIR correction are $J = 22.6$, $H = 23.2$, and $K_s = 23.6$ mag for SN 2010ma. The corrected measurements of the quasi-bolometric flux are presented in Fig. 8 for the GRB-SNe 2008hw, 2009nz, and 2010ma. For comparison, the quasi-bolometric light curves (340–2200 nm) for other SE SNe are also computed and plotted in Fig. 8. We note that all three events lie at a luminosity comparable to that of GRB-SNe 1998bw and 2006aj and are brighter than “normal” type-Ib/c SNe. Similar to the results we obtain for individual optical filters, SN 2010ma turns out to be brighter than SN 1998bw. The quasi-bolometric fluxes of SNe 2008hw, 2009nz, and 2010ma at maximum (Table 6) are comparable to $(1.07 \pm 0.07) \times 10^{43}$ erg s $^{-1}$ for SN 1998bw.

3.3.2. Physical parameters of the explosion

The nickel mass M_{Ni} , the ejected mass M_{ej} , and the kinetic energy E_k of the explosion were extracted from the luminosity models following the analytic approach by Arnett (1982) for ^{56}Ni -powered SNe (see e.g. Maeda et al. 2003; Taubenberger et al. 2006; Valenti et al. 2008; Pignata et al. 2011; Olivares E. et al. 2012; Roy et al. 2013). We therefore employed the following expression to model the bolometric luminosity:

$$L(t) = M_{\text{Ni}} e^{-x^2} \left[(\epsilon_{\text{Ni}} - \epsilon_{\text{Co}}) \int_0^x A(z) dz + \epsilon_{\text{Co}} \int_0^x B(z) dz \right], \quad (1)$$

where $A(z) = 2ze^{-2zy+z^2}$, $B(z) = 2ze^{-2zy+2zs+z^2}$, $x \equiv t/\tau_m$, $y \equiv \tau_m/(2\tau_{\text{Ni}})$, and $s \equiv \tau_m(\tau_{\text{Co}} - \tau_{\text{Ni}})/(2\tau_{\text{Co}}\tau_{\text{Ni}})$. The decay energy for ^{56}Ni and ^{56}Co are $\epsilon_{\text{Ni}} = 3.90 \times 10^{10}$ erg s $^{-1}$ g $^{-1}$ and $\epsilon_{\text{Co}} = 6.78 \times 10^9$ erg s $^{-1}$ g $^{-1}$, respectively (Sutherland & Wheeler 1984; Cappellaro et al. 1997). The decay times are $\tau_{\text{Ni}} = 8.77$ d and $\tau_{\text{Co}} = 111$ d. The timescale of the light curve is expressed as

$$\tau_m = \left(\frac{k_{\text{opt}}}{\beta c} \right)^{1/2} \left(\frac{6 M_{\text{ej}}^3}{5 E_k} \right)^{1/4}, \quad (2)$$

where $\beta \approx 13.8$ is an integration constant (Arnett 1982), c is the speed of light, and k_{opt} is the optical opacity, which stays constant in time for this modelling scheme. In reality, the opacity depends on the composition and temperature of the ejecta, therefore, it changes as the SN expands. Assuming a variable opacity, the models by Chugai (2000) for the bolometric light curve of SN 1998bw deliver an average value of 0.07 cm 2 g $^{-1}$ for the first 20 days after the explosion. The models by Mazzali et al. (2000) can reproduce the light curve of the type-Ic SN 1997ef at early times using a constant opacity of 0.08 cm 2 g $^{-1}$. With a constant opacity of 0.06 cm 2 g $^{-1}$, the synthetic light curves by Maeda et al. (2003) manage to reproduce the data of hypernovae at early phases. Thus, we choose a value of $k_{\text{opt}} = 0.07 \pm 0.01$ cm 2 g $^{-1}$, which includes within 1σ the opacity values that have been employed in the literature.

Equations (1) and (2) are valid only for the photospheric phase ($t - t_0 \lesssim 40$ d). Given the lack of detections beyond day 40, no nebular component has been considered (see appendix in Valenti et al. 2008, for the complete model). The modelling procedure employed consists of a weighted χ^2 minimisation, where M_{Ni} and M_{ej}^3/E_k are free. The latter will be dubbed the “timescale parameter” hereafter, because it approximates the light-curve shape (see Sect. 4 for details). To compute M_{ej} and E_k from the timescale parameter, we used the expression for the photospheric expansion velocity at maximum luminosity from Arnett (1982)³:

$$v_{\text{ph}}^2 \approx \frac{5}{3} \frac{2E_k}{M_{\text{ej}}}. \quad (3)$$

This quantity is critical to obtain reliable physical parameters of the explosion (Mazzali et al. 2013). A minimum expansion velocity of $\sim 14\,000$ km s $^{-1}$ (SN 1998bw; Pian et al. 2006) and a maximum of $\sim 28\,000$ km s $^{-1}$ (SN 2010bh; Bufano et al. 2012) have been measured for GRB-SNe. Thus, we employ $22\,000 \pm 4000$ km s $^{-1}$ if estimates of the photospheric velocity are not available. This conservative proxy encompasses with a 2σ confidence the photospheric velocity of most spectroscopically-confirmed GRB-SNe at maximum luminosity (see e.g. Bufano et al. 2012).

To calculate uncertainties, we performed one thousand Monte-Carlo simulations for each event. Assuming Gaussian errors, each simulation consisted of a χ^2 minimisation between the model with a randomised opacity and the randomised quasi-bolometric data. From the resulting distributions for M_{Ni} and M_{ej}^3/E_k , we obtained the median and the standard deviation (1σ). We then employed Eq. (3) to compute M_{ej} and E_k , propagating the errors accordingly. For SNe 2008hw and 2010ma, we computed the weighted average of M_{ej} and E_k using the proxy for the photospheric velocity as defined above. For SN 2009nz, Berger et al. (2011) measure an expansion velocity of $17\,000$ km s $^{-1}$ from Si II $\lambda 6355$, which has been identified as a reliable tracer of the photospheric velocity (Sauer et al. 2006; Valenti et al. 2008). Although the date of the spectrum (16.3 rest-frame days after the GRB) coincides quite well with the maximum luminosity, the spectral coverage barely extends to 6250 Å and the spectrum has low signal-to-noise ratio. Therefore, we assigned to this velocity a conservative uncertainty of 1500 km s $^{-1}$, which corresponds to about 30 Å. The physical parameters and best-fit models are listed and plotted in Table 6 and Fig. 8, respectively.

Figure 8 shows that the light curves are reasonably well modelled within the errors. In the case of SN 2009nz, however,

³ Arnett (1982) incorrectly uses a factor $3/5$ instead of $5/3$ in his Eq. (54) as explained in detail by Wheeler et al. (2014).

Table 6. Physical parameters from quasi-bolometric light curves.

SN	M_{Ni} [M_{\odot}]	M_{ej} [M_{\odot}]	E_k [10^{51} erg]	M_{ej}^3/E_k [$10^{-51} M_{\odot}^3 \text{erg}^{-1}$]	v_{ph} [10^3 km s^{-1}]	$\log L_{\text{max}}$ [erg s^{-1}]	t_{max} [days]	Reference
2008hw	$0.39^{+0.08}_{-0.04}$	$2.3^{+1.0}_{-0.7}$	$6.7^{+5.8}_{-5.2}$	$1.9^{+2.0}_{-0.6}$	22 ± 4	43.1 ± 0.3	12 ± 3	1
2009nz	0.50 ± 0.04	$2.4^{+0.6}_{-0.3}$	$4.1^{+1.6}_{-1.4}$	$3.3^{+1.8}_{-0.7}$	17 ± 1.5	43.0 ± 0.2	18 ± 4	1
2010ma	$0.43^{+0.03}_{-0.02}$	$1.3^{+0.4}_{-0.3}$	$3.6^{+2.2}_{-2.1}$	$0.6^{+0.3}_{-0.1}$	22 ± 4	43.1 ± 0.2	10 ± 2	1
1998bw	0.38–0.48 0.45 ± 0.01	11 3.4 ± 0.2	50 5.8 ± 1.0	27 6.6 ± 0.4	17 ± 1	43.03 ± 0.01	17.8	2, 3 1
2003dh	0.25–0.45	8	40	13	~ 20	~ 43.0	~ 18	4
2003lw	0.45–0.65	13	60	37	~ 18	~ 43.2	~ 18	5
2006aj	0.21 0.26 ± 0.01	2 0.6 ± 0.04	2 1.3 ± 0.2	4.0 0.16 ± 0.02	19 ± 1	42.99 ± 0.02	8.8	6, 7 1
2010bh	0.21 ± 0.03	2.6 ± 0.2	8.6 ± 2.5	2.0 ± 0.8	28	42.63	8.0	8, 9
2002ap	0.10	2.5	4	3.9	14	~ 42.4	~ 11	10
2003jd	0.36	3	7	3.9	13.5	~ 42.9	~ 17	11
2007uy	0.30 ± 0.01	4.4 ± 0.3	15 ± 1	5.6 ± 1.0	15.2	42.83	17.9	12
2008D	0.07–0.09	5.3 ± 1.0	6 ± 3	25 ± 17	~ 10	~ 42.4	~ 19	13, 14
2009bb	0.22 ± 0.06	4.1 ± 1.9	18 ± 7	3.8 ± 5.5	~ 20	~ 42.8	~ 18	15

Notes. Different parts of the table correspond to GRB-SNe analysed here (top), further GRB-SNe (middle), and other SE SNe (bottom). Uncertainties are given at the 1σ level. The v_{ph} values correspond to measurements as defined by Eq. (3). The L_{max} and t_{max} values are estimated at the maximum bolometric luminosity, where t_{max} is defined with respect to the explosion time.

References. (1) This paper; (2) Iwamoto et al. (1998); (3) Mazzali et al. (2001); (4) Mazzali et al. (2003); (5) Mazzali et al. (2006b); (6) Pian et al. (2006); (7) Mazzali et al. (2006a); (8) Olivares E. et al. (2012); (9) Bufano et al. (2012); (10) Mazzali et al. (2007); (11) Valenti et al. (2008); (12) Roy et al. (2013); (13) Mazzali et al. (2008); (14) Tanaka et al. (2009); (15) Pignata et al. (2011).

Berger et al. (2011) obtain a lower M_{Ni} ($0.35 M_{\odot}$ of ^{56}Ni). They scale the I -band photometry from Cobb et al. (2010c) to obtain a V -band absolute magnitude at maximum and then they compute M_{Ni} using a simplification of the formalism by Arnett (1982), which should deliver results similar to ours. Given that a higher ^{56}Ni mass implies higher luminosity (Colgate et al. 1980; Arnett 1982) and our data includes more flux (three GROND-bands plus the NIR correction), our value is likely more reliable. The M_{ej} quantity is consistent with that presented by Berger et al. (2011). Regarding SNe 2008hw and 2009nz, no detailed photometric studies have been published for these yet.

4. Discussion

Regarding the NIR correction utilised in Sect. 3, we have to address that the extrapolation to SNe with different properties is the major source of uncertainty for this correction, although the five SE SNe selected for the analysis already cover a wide range of properties. A clear case of deviation from our NIR correction is the contribution shown by SN 2002ap. Even though SN 2002ap was not preceded by a GRB, it was a type-Ic event that showed a maximum NIR fraction of about 0.6 of the total quasi-bolometric flux. Moreover, the colours of SN 2010ma turned out to be significantly bluer before $t < 20$ d than those of SN 1998bw. This could hint at a higher temperature of the SN envelope and, therefore, lower NIR fluxes. Therefore, we caution that there might be GRB-SNe that will not fit into our estimation of the NIR correction. The NIR fraction could have variations as large as ± 0.15 if we compare SN 2002ap to SN 2007uy. This would translate into a maximum variation of about $\pm 30\%$ in the quasi-bolometric flux (equivalent to a 1σ error of $\sim 10\%$) and therefore in the determinations of M_{Ni} . This issue could be solved in the future by using a larger sample i.e. by including observations of new GRB-SNe in the NIR-bands.

With the purpose of comparing the physical parameters computed by others for a set of different SNe, we gathered

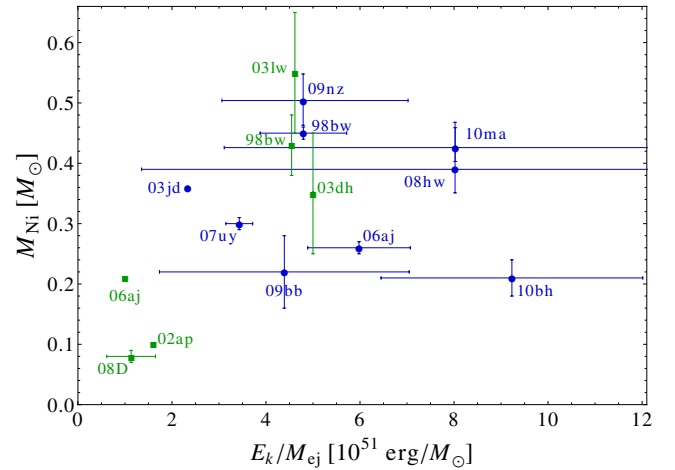


Fig. 9. Nickel mass against kinetic energy of the envelope per unit mass. While green squares depict values obtained via hydrodynamical simulations, blue circles correspond to parameters measured using the analytic approach by Arnett (1982). When ranges are given in Table 6, we plotted the weighted centre of the range. We caution that no uncertainties are available in the literature for some measurements (see Table 6).

results from the literature in Table 6, although uncertainties were unfortunately not available for all events. To compare the analytic method against the hydrodynamical simulations, we additionally computed the physical parameters of the explosion for SN 1998bw and SN 2006aj, using $v_{\text{ph}} = 17000$ and 19000 km s^{-1} (Pian et al. 2006), respectively. In Fig. 9 we plotted the kinetic energy per unit mass E_k/M_{ej} against the synthesised nickel mass M_{Ni} , a diagram that was presented by Bufano et al. (2012). The ratio E_k/M_{ej} is proportional to v_{ph}^2 (Eq. (3)), which is a common measurement for both the hydrodynamical and analytical approaches. Even though some values

have large uncertainties, we recognised a trend where the more energetic the SNe, the more ^{56}Ni it synthesises (Mazzali et al. 2007). We also note that hydrodynamical (green) and analytic (blue) measurements are inconsistent for SN 1998bw, despite showing similarities in M_{Ni} . The discrepancies in M_{ej} and E_{k} are probably attributed to (1) different values of k_{opt} ; (2) different values of ν_{ph} ; and (3) to the different assumptions intrinsic to the different approaches (hydrodynamical or analytic). This would also explain the smaller discrepancies shown for SN 2006aj, where the difference in M_{Ni} could be explained by our inclusion of the NIR data. We caution that especially the values obtained for M_{ej} and E_{k} might be highly model-dependent.

5. Summary and conclusions

Here we studied the GRB-SN connection by means of three individual events followed up in depth by XRT, UVOT, and GROND. The X-ray, UV, optical, and NIR data covered approximately six orders of magnitude in the radiative energy domain. Excluding γ -ray data, this represents a very comprehensive data set presented for the associations GRB 081007/SN 2008hw, GRB 091127/SN 2009nz, and GRB 101219B/SN 2010ma.

In Sect. 3, the light curves of the three events are thoroughly analysed. The host-galaxy extinction along the line of sight of each event is computed from the broad-band SED. The light curves of individual filter bands are modelled with SN 1998bw templates (Sect. 3.1). The AG component is subtracted to isolate the SN counterpart. The NIR flux was estimated from the data of five SE SNe and using BB fits of the optical data. This correction has been applied to the integrated optical flux of our rebrightenings to obtain quasi-bolometric light curves from 340 to 2200 nm. We note that the NIR contribution of SN 2002ap is 10–15% larger than that of the GRB-SNe 1998bw and 2006aj. Moreover, the colours of SN 2010ma at early times are bluer than those of SN 1998bw suggesting lower NIR fluxes for this object. Therefore, we conclude that more NIR data is needed to constrain the NIR contribution in GRB-SN light curves better. Using an analytic model for bolometric light curves, the physical parameters of the SN explosion were computed for each event analogous to the case of SN 2010bh in Olivares E. et al. (2012). We derived nickel and ejected masses of about 0.4–0.5 M_{\odot} and 1–3 M_{\odot} , respectively, and kinetic energies of about 10^{52} erg, which are higher than those of local type-Ic SNe and comparable to other GRB-SN events (see Table 6 and Fig. 9).

In conclusion, all three cases exhibit similarities to other GRB-SNe in terms of luminosity and physical parameters. SN 2008hw turned out to be somewhat fainter and slightly bluer than SN 1998bw (see Table 4). Moreover, SN 2009nz showed the most similarities with SN 1998bw in luminosity and evolution. SN 2010ma was significantly bluer and brighter than SN 1998bw. Both the latter and SN 2010bh have among the earliest optical peaks ever recorded (approximately eight days after the GRB) and fade more rapidly than almost every other GRB-SN, HN, or typical type-Ic SN.

Acknowledgements. We acknowledge the referee for suggestions and corrections that helped improve the paper significantly. F.O.E. thanks F. Bufano for sanity checks on the bolometric LCs. The Ph.D. studies of F.O.E. were funded both by the Deutscher Akademischer Austausch Dienst (DAAD) and the Comisión Nacional de Investigación Científica y Tecnológica (CONICYT). F.O.E. acknowledges support from FONDECYT through postdoctoral grant 3140326. F.O.E. and G.P. acknowledge support from project IC120009 “Millennium Institute of Astrophysics (MAS)” of the Iniciativa Científica Milenio del Ministerio de Economía, Fomento y Turismo de Chile. Part of the GROND funding (both hardware and personnel) was generously granted from the

Leibniz-Prize to Prof. G. Hasinger, Deutsche Forschungsgemeinschaft (DFG) grant HA 1850/28–1. S.K., A.R., A.N., D.A.K. acknowledge support by DFG grant KL 766/16-1. S.S. acknowledges support by the Thüringer Ministerium für Bildung, Wissenschaft und Kultur under FKZ 12010-514. D.A.K. acknowledges financial support from MPE and TLS. A.R., A.N., D.A.K. are grateful for travel funding support through MPE. This work made use of data supplied by the UK *Swift* Science Data Centre at the University of Leicester and data from the NASA’s Astrophysics Data System (NAS 5–26555). The Dark Cosmology Centre is funded by the Danish National Research Foundation.

References

- Arnett, D. 1996, *Supernovae and Nucleosynthesis* (New Jersey: Princeton University Press)
- Arnett, W. D. 1982, *ApJ*, **253**, 785
- Baade, W., & Zwicky, F. 1934, *Phys. Rev.*, **46**, 76
- Barthelmy, S. D., Barbier, L. M., Cummings, J. R., et al. 2005, *Space Sci. Rev.*, **120**, 143
- Baumgartner, W. H., Cummings, J. R., Evans, P. A., et al. 2008, *GCN Circ.*, **8330**, 1
- Berger, E., Fox, D. B., Cucchiara, A., & Cenko, S. B. 2008, *GCN Circ.*, **8335**, 1
- Berger, E., Chornock, R., Holmes, T. R., et al. 2011, *ApJ*, **743**, 204
- Beuermann, K., Hessman, F. V., Reinsch, K., et al. 1999, *A&A*, **352**, L26
- Bloom, J. S., Kulkarni, S. R., Price, P. A., et al. 2002, *ApJ*, **572**, L45
- Bolzonella, M., Miralles, J.-M., & Pelló, R. 2000, *A&A*, **363**, 476
- Bromberg, O., Nakar, E., Piran, T., & Sari, R. 2012, *ApJ*, **749**, 110
- Bucciantini, N., Quataert, E., Metzger, B. D., et al. 2009, *MNRAS*, **396**, 2038
- Bufano, F., Pian, E., Sollerman, J., et al. 2012, *ApJ*, **753**, 67
- Burrows, A. 2000, *Nature*, **403**, 727
- Burrows, D. N., Hill, J. E., Nousek, J. A., et al. 2005, *Space Sci. Rev.*, **120**, 165
- Cano, Z. 2013, *MNRAS*, **434**, 1098
- Cano, Z. 2014, *ApJ*, **794**, 121
- Cano, Z., & Jakobsson, P. 2014, *ApJ*, submitted [[arXiv:1409.3570](https://arxiv.org/abs/1409.3570)]
- Cano, Z., Bersier, D., Guidorzi, C., et al. 2011, *ApJ*, **740**, 41
- Cano, Z., de Ugarte Postigo, A., Pozanenko, A., et al. 2014, *A&A*, **568**, A19
- Cappellaro, E., Mazzali, P. A., Benetti, S., et al. 1997, *A&A*, **328**, 203
- Chornock, R., Berger, E., Levesque, E. M., et al. 2010, unpublished [[arXiv:1004.2262](https://arxiv.org/abs/1004.2262)].
- Chugai, N. N. 2000, *Astron. Lett.*, **26**, 797
- Clocchiatti, A., & Wheeler, J. C. 1997, *ApJ*, **491**, 375
- Cobb, B. E., Bloom, J. S., Cenko, S. B., & Perley, D. A. 2010a, *GCN Circ.*, **10400**, 1
- Cobb, B. E., Bloom, J. S., Morgan, A. N., Cenko, S. B., & Perley, D. A. 2010b, *CBET*, **2288**, 1
- Cobb, B. E., Bloom, J. S., Perley, D. A., et al. 2010c, *ApJ*, **718**, L150
- Colgate, S. A., Petschek, A. G., & Kriese, J. T. 1980, *ApJ*, **237**, L81
- Covino, S., Melandri, A., Salvaterra, R., et al. 2013, *MNRAS*, **432**, 1231
- Cucchiara, A., Fox, D., Levan, A., & Tanvir, N. 2009, *GCN Circ.*, **10202**, 1
- Cummings, J. R., Barthelmy, S. D., Baumgartner, W. H., et al. 2010, *GCN Circ.*, **11475**, 1
- de Ugarte Postigo, A., Thoene, C. C., & Gorosabel, J. 2012, *GCN Circ.*, **12802**, 1
- de Ugarte Postigo, A., Cano, Z., Thoene, C. C., et al. 2013, *CBET*, **3637**, 1
- Della Valle, M., Malesani, D., Benetti, S., et al. 2003, *A&A*, **406**, L33
- Della Valle, M., Malesani, D., Bloom, J. S., et al. 2006, *ApJ*, **642**, L103
- Della Valle, M., Benetti, S., Mazzali, P., et al. 2008, *CBET*, **1602**, 1
- Dessart, L., & Hillier, D. J. 2005, *A&A*, **439**, 671
- Dessart, L., Hillier, D. J., Waldman, R., Livne, E., & Blondin, S. 2012, *MNRAS*, **426**, L76
- Ferrero, P., Kann, D. A., Zeh, A., et al. 2006, *A&A*, **457**, 857
- Filgas, R., Greiner, J., Schady, P., et al. 2011, *A&A*, **535**, A57
- Filippenko, A. V. 1997, *ARA&A*, **35**, 309
- Folatelli, G., Bersten, M. C., Kuncarayakti, H., et al. 2014, *ApJ*, **792**, 7
- Foley, R. J., Papenkova, M. S., Swift, B. J., et al. 2003, *PASP*, **115**, 1220
- Fryer, C. L., Woosley, S. E., & Hartmann, D. H. 1999, *ApJ*, **526**, 152
- Fryer, C. L., Hungerford, A. L., & Young, P. A. 2007, *ApJ*, **662**, L55
- Galama, T. J., Vreeswijk, P. M., van Paradijs, J., et al. 1998, *Nature*, **395**, 670
- Galama, T. J., Tanvir, N., Vreeswijk, P. M., et al. 2000, *ApJ*, **536**, 185
- Gehrels, N., Chincarini, G., Giommi, P., et al. 2004, *ApJ*, **611**, 1005
- Gelbord, J. M., Barthelmy, S. D., Burrows, D. N., et al. 2010, *GCN Circ.*, **11473**, 1
- Golenetskii, S., Aptekar, R., Frederiks, D., et al. 2009, *GCN Circ.*, **10209**, 1
- Greiner, J., Klose, S., Salvato, M., et al. 2003, *ApJ*, **599**, 1223
- Greiner, J., Bornemann, W., Clemens, C., et al. 2007, *The Messenger*, **130**, 12
- Greiner, J., Bornemann, W., Clemens, C., et al. 2008, *PASP*, **120**, 405
- Greiner, J., Krühler, T., Klose, S., et al. 2011, *A&A*, **526**, A30
- Hansen, B. M. S. 1999, *ApJ*, **512**, L117

- Heger, A., Fryer, C. L., Woosley, S. E., Langer, N., & Hartmann, D. H. 2003, *ApJ*, **591**, 288
- Heise, J., in't Zand, J., Kippen, R. M., & Woods, P. M. 2001, in *Gamma-ray Bursts in the Afterglow Era*, eds. E. Costa, F. Frontera, & J. Hjorth, ESO Astrophys. Symp. (Rome, Italy: Springer-Verlag), 16
- Hjorth, J., & Bloom, J. S. 2012, *The Gamma-Ray Burst – Supernova Connection (CUP)*, 169
- Hjorth, J., Sollerman, J., Møller, P., et al. 2003, *Nature*, **423**, 847
- Iwamoto, K., Mazzali, P. A., Nomoto, K., et al. 1998, *Nature*, **395**, 672
- Jin, Z.-P., Covino, S., Della Valle, M., et al. 2013, *ApJ*, **774**, 114
- Kalberla, P. M. W., Burton, W. B., Hartmann, D., et al. 2005, *A&A*, **440**, 775
- Kann, D. A., Klose, S., Zhang, B., et al. 2010, *ApJ*, **720**, 1513
- Kann, D. A., Klose, S., Zhang, B., et al. 2011, *ApJ*, **734**, 96
- Kawabata, K. S., Deng, J., Wang, L., et al. 2003, *ApJ*, **593**, L19
- Kippen, R. M. 1998, *GCN Circ.*, **67**, 1
- Kippen, R. M., in't Zand, J. J. M., Woods, P. M., et al. 2004, in *Gamma-Ray Bursts: 30 Years of Discovery*, eds. E. Fenimore, & M. Galassi (Santa Fe, NM: AIP), *AIP Conf. Ser.*, **727**, 119
- Klose, S., Greiner, J., Fynbo, J., et al. 2012a, *GCN Circ.*, **13613**, 1
- Klose, S., Greiner, J., Fynbo, J., et al. 2012b, *CBET*, **3200**, 1
- Klose, S., Nicuesa Guelbenzu, A., Kruehler, T., et al. 2013, *CBET*, **3677**, 1
- Kocevski, D., Modjaz, M., Bloom, J. S., et al. 2007, *ApJ*, **663**, 1180
- Kouveliotou, C., Meegan, C. A., Fishman, G. J., et al. 1993, *ApJ*, **413**, L101
- Kouveliotou, C., Woosley, S. E., Patel, S. K., et al. 2004, *ApJ*, **608**, 872
- Li, X., & Hjorth, J. 2014, *A&A*, submitted [[arXiv:1407.3506](https://arxiv.org/abs/1407.3506)]
- Li, X., Hjorth, J., & Wojtak, R. 2014, *ApJ*, **796**, L4
- MacFadyen, A. I., & Woosley, S. E. 1999, *ApJ*, **524**, 262
- Maeda, K., Mazzali, P. A., Deng, J., et al. 2003, *ApJ*, **593**, 931
- Malesani, D., Tagliaferri, G., Chincarini, G., et al. 2004, *ApJ*, **609**, L5
- Markwardt, C. M., Barthelmy, S. D., Baumgartner, W. H., et al. 2008, *GCN Circ.*, **8338**, 1
- Masetti, N., Palazzi, E., Pian, E., et al. 2003, *A&A*, **404**, 465
- Matheson, T., Garnavich, P. M., Stanek, K. Z., et al. 2003, *ApJ*, **599**, 394
- Masetti, N., Palazzi, E., Pian, E., et al. 2005, *A&A*, **438**, 841
- Mazzali, P. A., Iwamoto, K., & Nomoto, K. 2000, *ApJ*, **545**, 407
- Mazzali, P. A., Nomoto, K., Patat, F., & Maeda, K. 2001, *ApJ*, **559**, 1047
- Mazzali, P. A., Deng, J., Tominaga, N., et al. 2003, *ApJ*, **599**, L95
- Mazzali, P. A., Deng, J., Nomoto, K., et al. 2006a, *Nature*, **442**, 1018
- Mazzali, P. A., Deng, J., Pian, E., et al. 2006b, *ApJ*, **645**, 1323
- Mazzali, P. A., Kawabata, K. S., Maeda, K., et al. 2007, *ApJ*, **670**, 592
- Mazzali, P. A., Valenti, S., Della Valle, M., et al. 2008, *Science*, **321**, 1185
- Mazzali, P. A., Walker, E. S., Pian, E., et al. 2013, *MNRAS*, **432**, 2463
- Mazzali, P. A., MacFadyen, A. I., Woosley, S. E., Pian, E., & Tanaka, M. 2014, *MNRAS*, **443**, 67
- Melandri, A., Pian, E., Ferrero, P., et al. 2012, *A&A*, **547**, A82
- Metzger, B. D., Giannios, D., Thompson, T. A., Bucciantini, N., & Quataert, E. 2011, *MNRAS*, **413**, 2031
- Minkowski, R. 1941, *PASP*, **53**, 224
- Modjaz, M., Stanek, K. Z., Garnavich, P. M., et al. 2006, *ApJ*, **645**, L21
- Modjaz, M., Li, W., Butler, N., et al. 2009, *ApJ*, **702**, 226
- Molinari, E., Vergani, S. D., Malesani, D., et al. 2007, *A&A*, **469**, L13
- Mould, J. R., Huchra, J. P., Freedman, W. L., et al. 2000, *ApJ*, **529**, 786
- Nomoto, K., Tanaka, M., Tominaga, N., & Maeda, K. 2010, *New Astron. Rev.*, **54**, 191
- Olivares E., F., Schady, P., Krühler, T., et al. 2011, *GCN Circ.*, **11578**, 1
- Olivares E., F., Greiner, J., Schady, P., et al. 2012, *A&A*, **539**, A76
- Paczynski, B. 1998a, *ApJ*, **494**, L45
- Paczynski, B. 1998b, in *Gamma-Ray Bursts: 4th Huntsville Symp.*, eds. C. A. Meegan, R. D. Preece, & T. M. Koshut, Huntsville, AL, *AIP Conf. Ser.*, **428**, 783
- Pastorello, A., Smartt, S. J., Botticella, M. T., et al. 2010, *ApJ*, **724**, L16
- Patat, F., Cappellaro, E., Danziger, J., et al. 2001, *ApJ*, **555**, 900
- Perley, D. A., Graham, M. L., Filippenko, A. V., & Cenko, S. B. 2014, *GCN Circ.*, **16454**, 1
- Pian, E., Antonelli, L. A., Piro, L., & Feroci, M. 1998, *GCN Circ.*, **158**, 1
- Pian, E., Amati, L., Antonelli, L. A., et al. 2000, *ApJ*, **536**, 778
- Pian, E., Mazzali, P. A., Masetti, N., et al. 2006, *Nature*, **442**, 1011
- Pignata, G., Stritzinger, M., Soderberg, A., et al. 2011, *ApJ*, **728**, 14
- Price, P. A., Kulkarni, S. R., Berger, E., et al. 2003, *ApJ*, **589**, 838
- Reichart, D. E., Lamb, D. Q., & Castander, F. J. 2000, in *Gamma-ray Bursts: 5th Huntsville Symp.*, eds. R. M. Kippen, R. S. Mallozzi, & G. J. Fishman (Huntsville, AL: AIP), *AIP Conf. Ser.*, **526**, 414
- Richardson, D. 2009, *AJ*, **137**, 347
- Riess, A. G., Macri, L., Casertano, S., et al. 2009, *ApJ*, **699**, 539
- Roming, P. W. A., Kennedy, T. E., Mason, K. O., et al. 2005, *Space Sci. Rev.*, **120**, 95
- Roy, R., Kumar, B., Maund, J. R., et al. 2013, *MNRAS*, **434**, 2032
- Sadler, E. M., Stathakis, R. A., Boyle, B. J., & Ekers, R. D. 1998, *IAU Circ.*, **6901**, 1
- Sakamoto, T., Hullinger, D., Sato, G., et al. 2008, *ApJ*, **679**, 570
- Sanders, N. E., Soderberg, A. M., Valenti, S., et al. 2012, *ApJ*, **756**, 184
- Sauer, D. N., Mazzali, P. A., Deng, J., et al. 2006, *MNRAS*, **369**, 1939
- Savaglio, S., Glazebrook, K., & Le Borgne, D. 2009, *ApJ*, **691**, 182
- Schady, P., Dwelly, T., Page, M. J., et al. 2012, *A&A*, **537**, A15
- Schlegel, D. J., Finkbeiner, D. P., & Davis, M. 1998, *ApJ*, **500**, 525
- Schulze, S., Leloudas, G., Xu, D., et al. 2013, *CBET*, **3587**, 1
- Schulze, S., Malesani, D., Cucchiara, A., et al. 2014, *A&A*, **566**, A102
- Skrutskie, M. F., Cutri, R. M., Stiening, R., et al. 2006, *AJ*, **131**, 1163
- Smith, N., Silverman, J. M., Filippenko, A. V., et al. 2012, *AJ*, **143**, 17
- Soderberg, A. M., Kulkarni, S. R., Price, P. A., et al. 2006, *ApJ*, **636**, 391
- Soderberg, A., Berger, E., & Fox, D. 2008, *GCN Circ.*, **8662**, 1
- Sollerman, J., Jaunsen, A. O., Fynbo, J. P. U., et al. 2006, *A&A*, **454**, 503
- Sparre, M., Fynbo, J., de Ugarte Postigo, A., Malesani, D., & Sollerman, J. 2011a, *CBET*, **2706**, 1
- Sparre, M., Sollerman, J., Fynbo, J. P. U., et al. 2011b, *ApJ*, **735**, L24
- Stamatikos, M., Barthelmy, S. D., Baumgartner, W. H., et al. 2009, *GCN Circ.*, **10197**, 1
- Stanek, K. Z., Matheson, T., Garnavich, P. M., et al. 2003, *ApJ*, **591**, L17
- Stanek, K. Z., Garnavich, P. M., Nutzman, P. A., et al. 2005, *ApJ*, **626**, L5
- Stritzinger, M., Mazzali, P., Phillips, M. M., et al. 2009, *ApJ*, **696**, 713
- Sutherland, P. G., & Wheeler, J. C. 1984, *ApJ*, **280**, 282
- Tanaka, M., Tominaga, N., Nomoto, K., et al. 2009, *ApJ*, **692**, 1131
- Taubenberger, S., Pastorello, A., Mazzali, P. A., et al. 2006, *MNRAS*, **371**, 1459
- Thöne, C. C., Goldoni, P., Covino, S., et al. 2009, *GCN Circ.*, **10233**, 1
- Thöne, C. C., de Ugarte Postigo, A., Fryer, C. L., et al. 2011, *Nature*, **480**, 72
- Troja, E., Barthelmy, S. D., Baumgartner, W. H., et al. 2009, *GCN Circ.*, **10191**, 1
- Troja, E., Sakamoto, T., Guidorzi, C., et al. 2012, *ApJ*, **761**, 50
- Udike, A., Rossi, A., Rau, A., et al. 2009, *GCN Circ.*, **10195**, 1
- Valenti, S., Benetti, S., Cappellaro, E., et al. 2008, *MNRAS*, **383**, 1485
- van der Horst, A. J. 2010, *GCN Circ.*, **11477**, 1
- van Paradijs, J., Kouveliotou, C., & Wijers, R. A. M. J. 2000, *ARA&A*, **38**, 379
- Vergani, S. D., Flores, H., Covino, S., et al. 2011, *A&A*, **535**, A127
- Wheeler, J. C., Johnson, V., & Clocchiatti, A. 2014, *MNRAS*, submitted [[arXiv:1411.5975](https://arxiv.org/abs/1411.5975)]
- Woosley, S. E. 1993, *ApJ*, **405**, 273
- Woosley, S. E. 2010, *ApJ*, **719**, L204
- Woosley, S. E., & Bloom, J. S. 2006, *ARA&A*, **44**, 507
- Woosley, S. E., & MacFadyen, A. I. 1999, *A&AS*, **138**, 499
- Xu, D., de Ugarte Postigo, A., Leloudas, G., et al. 2013, *ApJ*, **776**, 98
- Yoshii, Y., Tomita, H., Kobayashi, Y., et al. 2003, *ApJ*, **592**, 467
- Zeh, A., Klose, S., & Hartmann, D. H. 2004, *ApJ*, **609**, 952
- Zhang, B., & Mészáros, P. 2004, *Int. J. Mod. Phys. A*, **19**, 2385
- Zhang, B., Zhang, B. B., Virgili, F. J., et al. 2009, *ApJ*, **703**, 1696

Appendix A: Optical/NIR photometry

The three tables presented as follows are corrected for Galactic foreground extinction (Schlegel et al. 1998).

Table A.1. GRB 081007/SN 2008hw.

$t - t_0$ [d]	Δt^a [ks]	g'	r'	i'	z'	$t - t_0$ [d]	Δt [ks]	J	H	K_s
0.013	0.39	17.25(16)	17.28(11)	17.14(09)	17.02(08)	0.013	0.40	17.22(05)	16.76(03)	16.56(05)
0.018	0.40	17.51(16)	17.53(11)	17.37(09)	17.29(08)	0.019	0.42	17.53(05)	17.06(03)	16.82(04)
0.025	0.69	17.77(16)	17.78(11)	17.64(09)	17.53(07)	0.026	0.75	17.77(05)	17.28(03)	17.05(04)
0.035	0.70	17.99(16)	17.92(11)	17.85(09)	17.76(08)	0.035	0.76	17.98(05)	17.44(05)	17.26(04)
0.050	1.74	18.28(16)	18.18(11)	18.11(09)	17.96(07)	0.050	1.79	18.16(05)	17.70(03)	17.51(04)
0.071	1.75	18.51(16)	18.48(11)	18.34(09)	18.25(07)	0.071	1.80	18.39(05)	17.94(04)	17.74(04)
0.092	1.72	18.68(16)	18.67(11)	18.57(09)	18.50(07)	0.092	1.77	18.58(05)	18.10(04)	17.90(05)
0.912	2.53	20.42(16)	20.29(13)	20.15(10)	20.03(08)	0.902	0.75	20.11(07)	>19.41	>19.16
3.807	1.73	22.00(34)	22.09(27)	21.99(28)	21.88(28)	0.917	1.79	20.20(06)	19.59(10)	19.54(10)
10.85	5.33	>23.46	23.32(15)	22.99(23)	23.17(25)	3.808	1.78	>20.96	>20.03	>19.24
15.91	5.32	>23.87	23.17(20)	23.20(35)	>22.43	10.85	5.37	>21.67	>20.84	>19.44
18.83	7.17	>23.75	23.27(30)	22.97(32)	22.76(31)	15.91	5.38	>21.67	>20.76	>19.83
22.86	7.11	>24.03	23.51(25)	23.45(38)	23.15(36)	18.83	7.21	>21.15	>19.67	>19.62
28.89	3.53	>23.29	>22.78	>22.18	>21.12	22.86	7.16	>21.43	>20.69	>20.00

Notes. The GRB trigger time is $t_0 = 54\,746.225$ MJD. All data corrected for $A_{V,\text{host}} = 0.68 \pm 0.08$ mag (SMC). Image subtraction of the host was performed for $g'r'i'z'$. ^(a) The duration of the observation.

Table A.2. GRB 091127/SN 2009nz.

$t - t_0$ [d]	Δt^a [ks]	g'	r'	i'	z'	$t - t_0$ [d]	Δt [ks]	J	H
1.075	1.55	19.69(03)	19.50(05)	19.37(03)	19.17(01)	1.070	0.75	19.04(08)	18.81(09)
...	1.080	0.73	19.09(08)	18.88(09)
1.260	0.69	19.94(03)	19.77(03)	19.69(03)	19.46(03)	1.243	1.75	19.23(06)	18.99(07)
2.079	1.70	20.81(04)	20.58(04)	20.47(01)	20.38(02)	2.080	1.75	20.09(09)	19.86(10)
2.198	1.71	20.88(03)	20.65(04)	20.54(03)	20.41(03)	2.198	1.77	20.09(07)	19.90(12)
3.207	1.71	21.64(07)	21.32(04)	21.26(05)	21.13(05)	3.207	1.76	20.54(32)	20.52(22)
4.212	1.70	22.10(09)	21.87(06)	21.85(10)	21.60(07)	4.212	1.75	20.88(18)	20.99(28)
6.175	1.71	22.68(13)	22.40(10)	22.51(14)	22.22(10)	6.175	1.75	21.53(31)	>21.26
11.10	1.71	23.76(12)	22.76(06)	22.50(10)	22.86(13)	11.10	1.75	>21.63	>21.16
23.17	0.34	>22.87	22.85(23)	>22.05	>22.15
46.13	3.92	>24.43	24.08(13)	23.58(27)	23.20(22)	46.13	3.97	21.74(27)	>21.35
49.12	1.70	>24.69	24.49(32)	>23.41	23.28(26)	49.12	1.75	>21.69	>21.19
54.09	1.90	>21.26	>23.88	>18.86	>22.51	54.09	1.75	>21.37	>20.93

Notes. The GRB trigger time is $t_0 = 55\,162.976$ MJD. Data not corrected for negligible $A_{V,\text{host}} < 0.03$ mag (LMC). Image subtraction of the host was performed for $g'r'i'z'$. ^(a) The duration of the observation.

Table A.3. GRB 101219B/SN 2010ma.

$t - t_0$ [d]	Δt^a [ks]	g'	r'	i'	z'	$t - t_0$ [d]	Δt [ks]	J	H	K_s
0.342	0.91	19.71(05)	19.60(05)	19.58(06)	19.33(07)	0.342	0.92	19.10(09)	19.02(12)	18.73(23)
0.356	1.44	19.78(05)	19.73(03)	19.57(03)	19.54(04)	0.357	1.49	19.26(08)	19.08(11)	18.84(20)
0.376	1.71	19.81(06)	19.77(02)	19.63(03)	19.57(03)	0.376	1.76	19.33(07)	18.98(10)	19.07(26)
0.446	1.72	20.00(06)	19.90(04)	19.73(03)	19.76(04)	0.447	1.77	19.61(10)	19.31(12)	18.74(23)
1.353	2.92	21.13(09)	21.09(04)	20.97(05)	20.99(07)	1.354	2.98	21.06(22)	20.64(21)	19.88(37)
2.381	1.47	21.76(17)	21.67(07)	21.72(09)	21.87(15)	6.442	4.20	21.44(39)	21.06(44)	>19.60
2.508	1.61	>21.86	>22.30	>22.02	>21.83	2.381	1.52	>20.95	21.05(30)	>19.11
3.387	1.72	22.36(17)	22.05(07)	22.05(10)	22.29(13)	2.507	1.52	>20.43	>19.96	>19.81
5.399	3.53	22.64(05)	22.26(05)	22.27(06)	22.53(16)	3.388	1.77	>21.10	>20.80	>20.04
6.445	3.53	22.99(10)	22.49(09)	22.46(10)	22.78(28)	5.399	3.58	>21.38	>20.74	>19.71
9.395	6.69	23.17(06)	22.41(04)	22.23(08)	22.93(17)	9.377	3.58	>21.10	>20.77	>19.98
10.38	3.52	23.07(12)	22.49(07)	22.34(11)	22.83(17)	10.38	3.56	>21.37	>21.03	>20.21
12.38	3.52	23.39(07)	22.55(06)	22.35(09)	22.89(17)	12.38	3.57	>21.30	>20.79	>20.17
14.39	3.52	23.31(17)	22.61(15)	22.71(17)	22.85(28)	14.39	3.57	>20.67	>20.34	>19.13
16.41	6.71	23.67(19)	22.83(05)	22.46(16)	22.85(24)	16.40	3.59	>20.95	>20.38	...
24.37	4.18	>23.72	23.23(15)	22.72(18)	23.00(20)	24.37	4.23	>21.28	>20.67	>19.35
26.35	0.78	>22.36	>22.79	>21.57	>21.59	26.35	0.83	>20.35	>20.11	>19.50
26.43	9.85	>23.95	23.72(16)	22.77(13)	22.84(19)	26.44	4.94	>21.71	>21.19	>19.84
35.44	4.88	>24.46	23.75(11)	23.28(14)	23.60(34)	35.44	4.93	>21.44	>21.08	>19.47

Notes. The GRB trigger time is $t_0 = 55\,549.686$ MJD. All data corrected for $A_{V,\text{host}} = 0.12 \pm 0.01$ mag (SMC). ^(a) The duration of the observation.

Appendix B: Sequences of standard stars

The sequence of reference stars in the field of GRB 091127/SN 2009nz are taken from [Filgas et al. \(2011\)](#). Stars from the 2MASS catalogue ([Skrutskie et al. 2006](#)) are used for the JHK_s -bands.

Table B.1. Reference stars in the field of GRB 081007/SN 2008hw.

RA [°]	Dec [°]	g'	r'	i'	z'
339.91132	−40.14995	19.334 ± 0.013	18.940 ± 0.011	18.795 ± 0.016	18.658 ± 0.017
339.91385	−40.15378	19.050 ± 0.011	18.495 ± 0.007	18.274 ± 0.012	18.075 ± 0.012
339.92912	−40.17095	14.897 ± 0.001	14.399 ± 0.001	14.220 ± 0.001	14.091 ± 0.001
339.94805	−40.15443	...	19.887 ± 0.020	18.788 ± 0.016	18.285 ± 0.014
339.95393	−40.11101	19.971 ± 0.020	19.147 ± 0.011	18.807 ± 0.016	18.641 ± 0.018
339.97304	−40.11895	19.890 ± 0.019	19.201 ± 0.012
339.97329	−40.17987	19.631 ± 0.016	18.129 ± 0.006	16.949 ± 0.005	16.399 ± 0.004
339.98310	−40.12094	19.542 ± 0.015	18.780 ± 0.009	18.488 ± 0.013	18.309 ± 0.014
339.99130	−40.17932	17.947 ± 0.005	17.691 ± 0.004	17.588 ± 0.007	17.517 ± 0.007

Notes. All are observed magnitudes in the AB system.

Table B.2. Reference stars in the field of GRB 101219B/SN 2010ma.

RA [°]	Dec [°]	g'	r'	i'	z'
12.22124	−34.52946	22.85 ± 0.10	19.87 ± 0.05	18.365 ± 0.019	17.720 ± 0.018
12.25499	−34.54326	19.021 ± 0.031	18.006 ± 0.011	17.568 ± 0.012	17.368 ± 0.015
12.26985	−34.56368	21.02 ± 0.07	19.519 ± 0.034	18.475 ± 0.022	18.088 ± 0.025
12.22871	−34.56753	15.350 ± 0.003	14.928 ± 0.002	14.772 ± 0.002	14.674 ± 0.003
12.24608	−34.57123	17.328 ± 0.010	17.099 ± 0.006	17.017 ± 0.009	16.970 ± 0.011
12.21783	−34.57419	20.41 ± 0.06	19.226 ± 0.029	18.663 ± 0.026	18.484 ± 0.039
12.26934	−34.58304	16.972 ± 0.007	16.599 ± 0.004	16.446 ± 0.006	16.398 ± 0.007
12.25056	−34.58787	16.996 ± 0.007	15.583 ± 0.003	14.623 ± 0.002	14.166 ± 0.002
12.21137	−34.59066	18.380 ± 0.017	18.173 ± 0.013	18.097 ± 0.016	18.125 ± 0.027

Notes. All are observed magnitudes in the AB system.

Appendix C: Black-body fits

Here we present the black-body fits for the analysed GRB-SNe, which were utilised to estimate the NIR contribution (Sect. 3.3.1).

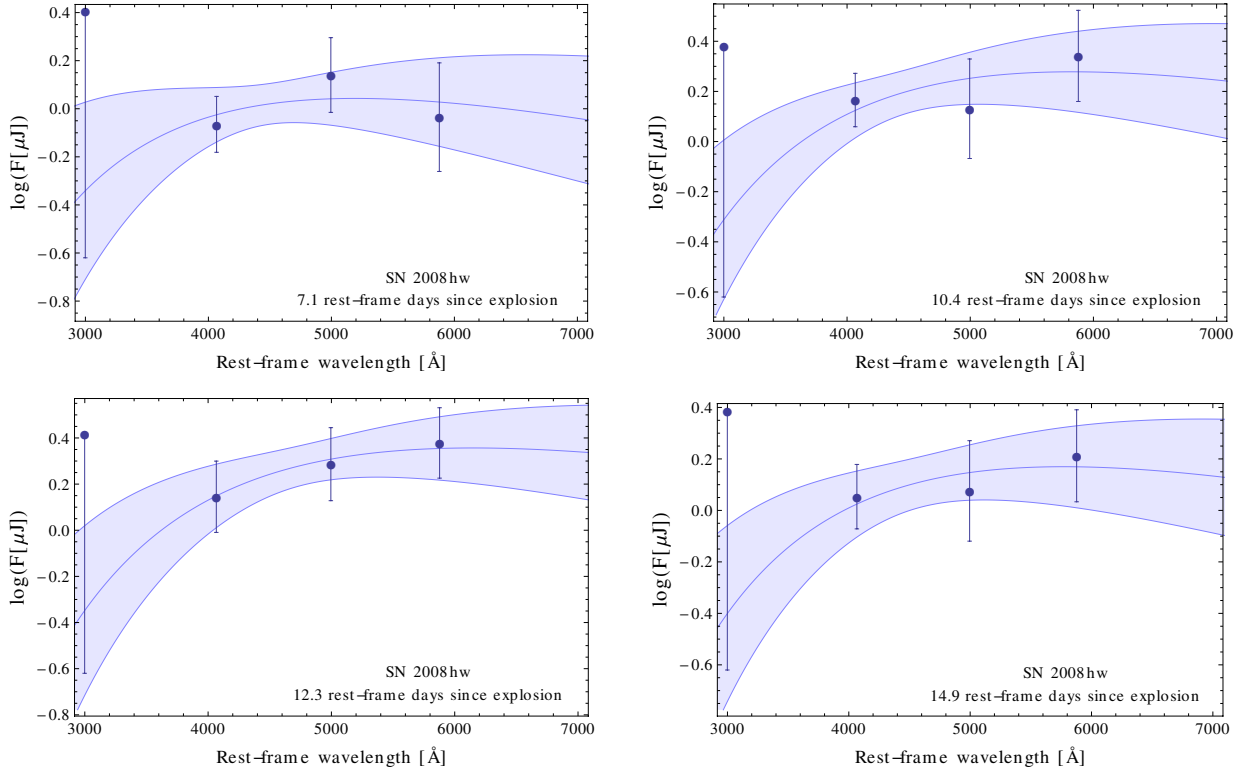


Fig. C.1. Black-body fits to the optical photometry of SN 2008hw. Colour temperatures are about 5000 K. Points with only a lower error bar are upper limits. The blue shaded region shows the area between the 1σ contours, where the central line is the best fit.

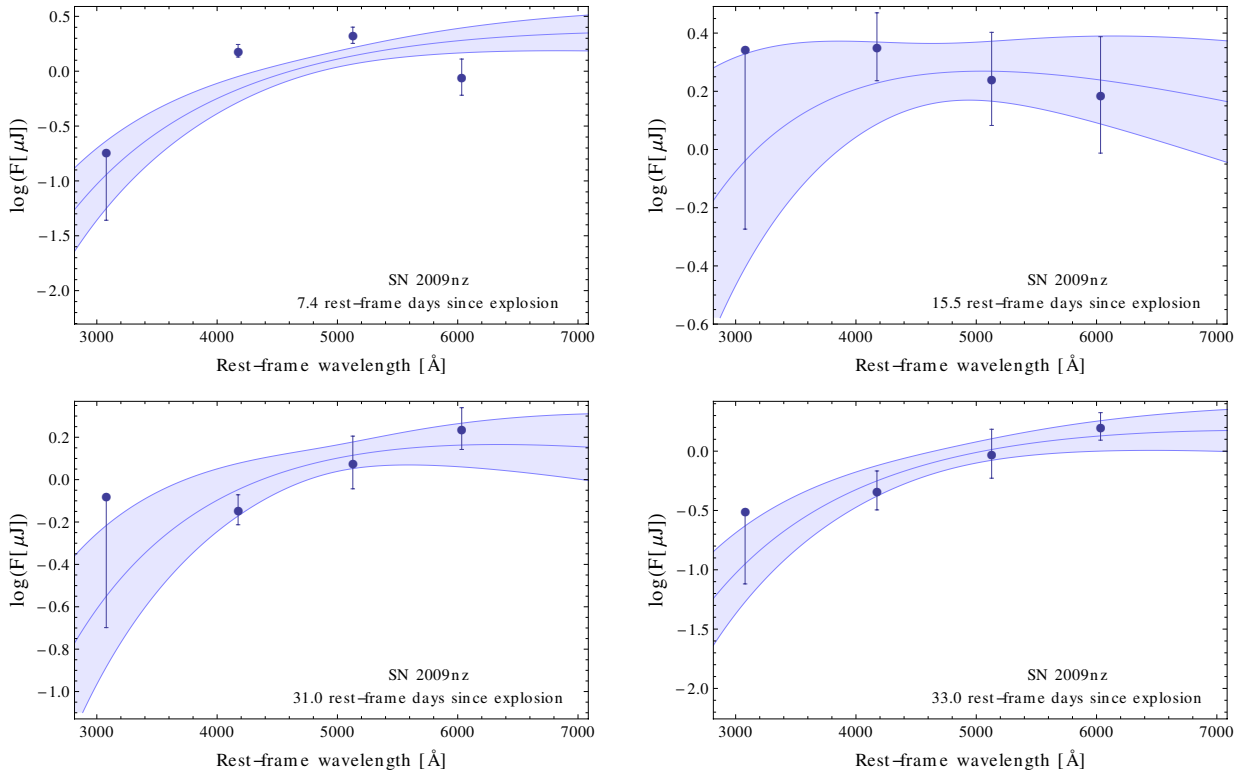


Fig. C.2. Black-body fits to the optical photometry of SN 2009nz. Colour temperatures evolve from ~ 7000 to ~ 4000 K approximately. Point, line, and region coding are the same as in Fig. C.1.

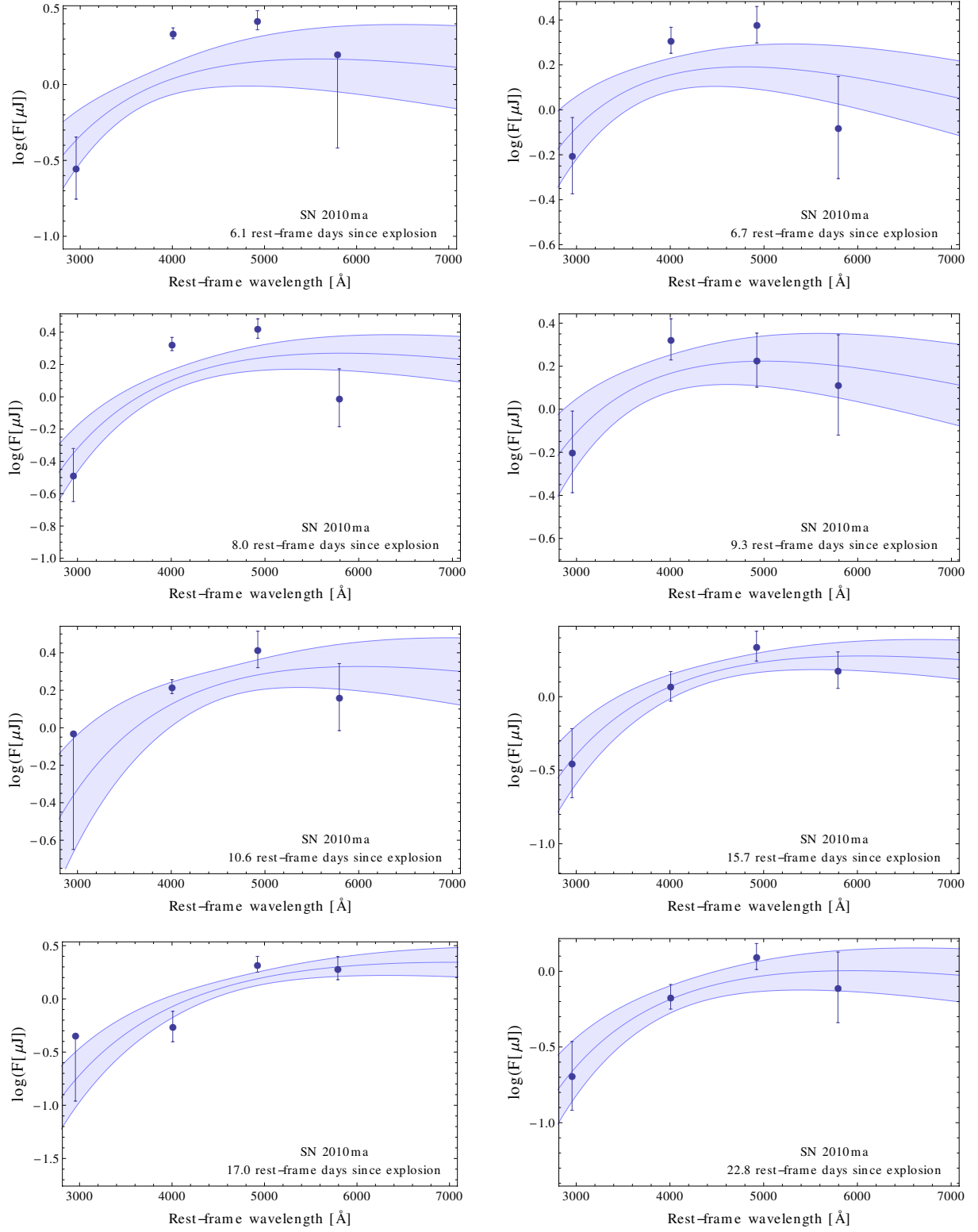


Fig. C.3. Black-body fits to the optical photometry of SN 2010ma. Colour temperatures evolve from ~ 6000 to ~ 4000 K. Point, line, and region coding are the same as in Fig. C.1.